AN ABSTRACT OF THE THESIS OF

DONALD JAMES LYNCH for the DOCTOR OF PHILOSOPHY
(Name of student) (Degree)

in Physics presented on July 6, 1971
(Major) June 1972
(Date)

TITLE: OBSERVATION OF FINE STRUCTURE INTERFERENCE EFFECTS IN LYMAN-BETA RADIATION FROM BEAM-FOIL EXCITED HYDROGEN ATOMS

Redacted for privacy

Abstract approved: _____
Dr. Charles W. Drake

Zero-field quantum beats were observed in Lyman-Beta emission from hydrogen atoms formed by beam-foil excitation. The energy dependence of the magnetic substate relative cross sections for the n=3, L=1 states of H was determined for beam energies in the range from 230 to 500 keV per atom. The theoretical values of the fine structure energy splitting and the natural lifetime of the $3p_{1/2}$ and $3p_{3/2}$ states were verified.

Observation of Fine Structure Interference Effects in Lyman-Beta Radiation from Beam-Foil Excited Hydrogen Atoms

by

Donald James Lynch

A THESIS

submitted to

Oregon State University

in partial fulfillment of
the requirements for the
degree of

Doctor of Philosophy

June 1972

APPROVED:

Redacted for privacy

Associate Professor of Physics
in charge of major

Redacted for privacy

Chairman of Department of Physics

Redacted for privacy

Dean of the Graduate School

Date thesis is presented July 6, 1971

Typed by Opal Grossnicklaus for Donald James Lynch

ACKNOWLEDGEMENT

It is a pleasure to acknowledge those who have directly contributed to the completion of this study. Professor Charles W. Drake has provided continuous support and encouragement in all phases of my research. Professor Clifford Fairchild and Mr. Mark Alguard have actively participated in the beam-foil experiments. The latter also deserves thanks for his contributions to the data reduction and analysis of this work. The Research Corporation has provided financial support through a Cottrell Grant to Dr. Drake. Appreciation is also expressed for a National Defense Education Act Fellowship which was awarded to me by Oregon State University. The Nuclear Physics Group at the University of Oregon has generously supported this project. Finally, my wife, Lenore, deserves special thanks for both her moral support and her clerical assistance.

TABLE OF CONTENTS

LIST OF FIGURES

LIST OF TABLES

OBSERVATION OF FINE STRUCTURE INTERFERENCE EFFECTS IN LYMAN-BETA RADIATION FROM BEAM-FOIL EXCITED HYDROGEN ATOMS

INTRODUCTION

Because of its fundamental nature, atomic hydrogen has been the subject of extensive study, both experimentally and theoretically, for many years (1). Its measured properties serve to test various theories involving atomic interactions which apply to more complicated atoms as well. The process to be studied in this dissertation involves the passage of a high energy beam of hydrogen ions through a thin foil target (2). In passing through the foil, some of the ions capture electrons, thus forming atoms. The radiative decay of excited states of foil-excited hydrogen atoms is investigated here.

The foil target is thin in the sense that an incident ion traverses the foil in a time on the order of 10^{-15} seconds which is short compared to atomic lifetimes. It is thick in the sense that many interactions of the target particles and the incident ions take place during the passage of the ions through the foil (3, 4). At the present time there is no detailed theoretical description of the beam-foil collision mechanism. Nonetheless, some of the qualitative features of this process have been discussed.

It has been shown that excited atomic states created deep within the foil have a negligible probability of emerging (3). This

implies that only those excited states which are created in the last few monolayers of the foil will emerge. These arguments make plausible the notion that the dominant contribution to the formation of an excited state of an atom emerging from a foil will be the direct capture of electrons into the excited state on the exit surface layer of the target (3). On the other hand, the charge state distribution of a beam emerging from the foil has been shown to be dependent on the internal atoms in the foil, and not just the surface (4).

The primary advantage of the beam-foil method of excitation of atomic states compared to the gas target method (5) used in ion-atom collisions is that the position along the beam axis at which the formation of excited states occurs is well defined. The resulting time resolution for a known beam velocity allows for the measurement of the radiative properties of excited states of ions as well as neutral atoms.

Although the gross features of the decay of foil-excited atoms have been understood for some time (2), it has only recently been realized that this method of excitation allows for a more detailed investigation of the decaying states (6). Interference effects arising from the decay of coherent fine structure states in an excited level provide a means of studying the properties of the excitation process and the excited levels themselves (6). In the present work, relative total cross sections for the formation of orbital angular momentum

magnetic substates are determined for the n=3, L=1 states of atomic hydrogen at various beam energies. Additionally, the theoretical values of the fine structure energy splitting and the natural lifetime of these states are verified experimentally.

THEORY OF THE EXPERIMENT

The Beam-Foil Method

The basis of the present experiment is the beam-foil method of excitation of atoms. In this method (2, 7), ions of some element of interest are accelerated, energy analyzed with a bending magnet, and directed into an evacuated target chamber. Typically, the target is a thin carbon foil which is in a plane perpendicular to the beam axis. The ions pass through the foil, undergo interactions therein, and the interaction products--neutral atoms and ions in various charge states--emerge from the foil with a well determined velocity. Light is emitted in the radiative decay of excited states of the various interaction products.

Since the foil is thin (200 to 2000 Å thick), the position along the beam axis where the excitations occur is well defined. If a spectral line corresponding to the transition from a particular energy level to a lower level is isolated by means of a spectrometer or an interference filter, its intensity is related to the number of particles in the upper level. As the excited particles move downstream from the foil, the intensity of each emission line decreases. Because the particle speeds are constant, the variation of intensity with distance determines the variation of intensity with time, and the former thus measures the time dependence of the decaying level. This means

that the measurement of the intensity of a spectral line versus distance can be directly interpreted in terms of the mean life of the decaying state. Beam velocities are typically 10^7 to 10^9 cm/sec so that lifetimes in the range 10^{-10} to 10^{-7} seconds are resolvable.

The population of any given state not only is decreased by radiative decay, but also is augmented by transitions from higher energy states. The effect of such cascading must be taken into account in analyzing the decay of a particular level (8).

Theory of Zero Field Quantum Beats

It was first pointed out by Macek (6, 9) that the usual description of beam-foil excitation of atomic levels, as discussed above, assumes that the eigenstates of a free atom are incoherently excited by the beam-foil interaction. He showed that, in principle, interference effects produced by coherence in the excitation of fine structure states should be observed in the radiative decay of excited levels under certain conditions, to be discussed below.

We denote atomic states by the indices a, j and m, where j is the total angular momentum of the atom, m is its projection onto the quantization axis, which usually is chosen to be the beam axis in a beam-foil experiment, and "a" denotes all other quantum numbers. Consider a group of upper levels with quantum numbers a_1, j_1 and m_1 which are degenerate in the magnetic quantum number m_1 but

non-degenerate in j_1. The upper levels decay to a group of lower levels a_o, j_o, m_o via electric dipole transitions. In a beam-foil collision the upper states are populated in a time of the order of 10^{-15} seconds which is much shorter than typical decay times ($\sim 10^{-9}$ seconds). Thus, the excited states are populated according to the excitation amplitudes $A(a_1, j_1, m_1)$ at $t = 0$. The time derivative of the probability $P_q(t)$ for finding an atom in one of the lower levels a_o, j_o, m_o and photon of polarization q and angular frequency ω_o in surrounding space is (9)

$$\dot{P}_q(t) = K \sum_{1,1',o} A(a_1, j_1, m_1) \cdot (a_1\, j_1\, m_1 | X_q | a_o j_o m_o)$$

$$\cdot A^*(a_1', j_1', m_1') \cdot (a_1' j_1' m_1' | X_q | a_o j_o m_o)^* \cdot \exp\{[-i\omega_{1,1'} - \frac{(\gamma_1 + \gamma_1')}{2}]t\} \qquad (1)$$

where $K = 4e^2\omega_o^2/3c^3$, $\sum_{1,1',o}$ is shorthand for $\sum_{a_1 j_1 m_1,\, a_1' j_1' m_1',\, a_o j_o m_o}$, X_q is the qth component of the electric dipole operator, $\hbar\omega_{1,1'}$ is the energy separation of a_1, j_1, m_1 and a_1', j_1', m_1', and γ_1 is the radiative decay constant of the state a_1, j_1, m_1. The energy splitting of the excited states has been neglected in comparison with the energy of the excited levels above the ground level ($\omega_{1,o} \simeq \omega_{1,o}' \simeq \omega_o$). This equation is the fundamental expression for the theory of radiative decay measurements. The amplitudes $A(a_1, j_1, m_1)$ contain all the information about the excitation of the upper states in the atomic collision.

It should be noted that, thus far, no assumptions have been made concerning the properties of the excitation amplitudes.

Eq. 1 is obtained (9) by integrating, over all photon frequencies and directions, the probability for finding the atom, at time t, in a lower state, a_o, j_o, m_o, and a photon in the surrounding field, given the initial condition that the atom is in an upper state, a_1, j_1, m_1, at $t = 0$. Differentiating the resulting expression with respect to time gives Eq. 1 directly. The significant point to be made is that an integration over photon frequencies has been performed. Interference effects, contained in the cross terms $(a_1, j_1, m_1 \neq a_1', j_1', m_1')$ in Eq. 1, arise because of this integration. In relating this expression to experiments which measure photon intensities, we require that the photon detection be independent of $\omega_{1,o}$ over a range $\Delta\omega$ greater than $\omega_{1,1'}$.

The upper states a_1, j_1, m_1 and a_1', j_1', m_1' are coherent if there is a definite (non-random) phase relation between the corresponding probability amplitudes $A(a_1, j_1, m_1)$ and $A(a_1', j_1', m_1')$. Macek (10) has pointed out that, in general, the relative phases of the probability amplitudes for the basis states of any complete set in which we expand the wave function of the beam ion-foil system are non-random. Only the eigenstates of the collision Hamiltonian for the beam-foil system form a basis in which the probability amplitudes have random phase. Since the Hamiltonian for the free atom plus

foil system after collision is not the collision Hamiltonian, we expect the probability amplitudes in Eq. 1 to have non-random phase relations. The subsequent interference effects appear as sinusoidal oscillations in the intensity of the radiative decay of the upper states a_1, j_1, m_1 and a_1', j_1', m_1' to the common lower state a_o, j_o, m_o. The frequency of the oscillations corresponds to the energy separation of the excited states.

In order to simplify the discussion of the excitation amplitudes, we will neglect hyperfine structure at this point. The effect of hyperfine structure will be discussed below. In addition, the present development is restricted to the radiative decay of hydrogen atoms from excited states to the ground state. The states a, j, m are thus n, L, S, J, M_J, where n is the principle quantum number of the atomic level, and L, S, J and M_J are the orbital angular momentum, spin angular momentum, total angular momentum, and its magnetic projection quantum numbers, respectively, for the eigenstates of the atom after it emerges from the foil.

Since electrostatic forces dominate the interaction of a beam atom with the foil and since the time an atom spends in the foil is short compared to the period associated with the energy splittings of fine structure levels, we include only electrostatic interactions in the collision Hamiltonian for each atom. These simplifications give rise to the following picture of the excitation and decay process.

An atom is initially excited into a linear combination of orbital angular momentum states. Once the atom is formed, the fine structure interaction acts as a perturbation of the Coulomb Hamiltonian of the free atom, yielding atomic eigenstates of total angular momentum, which are linear combinations of the orbital angular momentum states. Those total angular momentum states which contain admixtures of the same orbital angular momentum state are coherent, and therefore, interfere in decaying to a common ground state.

The probability amplitudes $U(n, L, M_L, S, M_S)$ for excitation of orbital angular momentum states are related to the amplitudes $A(n, L, S, J, M_J)$ of the total angular momentum states by the following relation.

$$A(n, L, S, J, M_J) = \sum_{M_L M_S} U(n, L, M_L, S, M_S)\ C(LSJ; M_L M_S M_J) \tag{2}$$

where the C's are the Clebsh-Gordon angular momentum coupling coefficients.

If hydrogen atoms are excited, and subsequently decay to the ground state, which has orbital angular momentum $L_O = 0$, only excited states with $L_1 = 1$ contribute to the intensity since the electric dipole transition matrix element contains the selection rule $\Delta L = \pm 1$ (1). Furthermore, cylindrical symmetry about the beam axis implies (9) that M_L is a good quantum number of the collision Hamiltonian. This leads to the result that the orbital angular momentum magnetic

substates are incoherently excited, meaning there is an arbitrary phase factor between the probability amplitudes of different M_L states. When Eq. 2 is inserted into Eq. 1 and the above restrictions are imposed, the expression for the total intensity of the polarization q and angular frequency ω_o is (9)

$$I_q \propto \{ \sum_{l,l',o\,(L_l = L_l' = 1,\ L_o = 0)} \langle n_l L_l S_l J_l M_{J_l} | Xq | n_o L_o S_o J_o M_{J_o} \rangle \langle n_l' L_l' S_l' J_l' M_{J_l'} | Xq | n_o L_o S_o J_o M_{J_o} \rangle^* \cdot \exp\left[\left(-i\omega_{l,l'} - \frac{\gamma_l + \gamma_l'}{2}\right)t\right] \cdot \sum_{M_{L_l} M_{S_l}} C(L_l S_l J_l; M_{L_l} M_{S_l}, M_{J_l})\, C(L_l S_l J_l'; M_{L_l} M_{S_l} M_{J_l'})\, \sigma_{M_{L_l}} \} \quad (3)$$

where $\sigma_{M_{L_l}} = |U(n_l, L_l = 1, M_{L_l}, S_l, M_{S_l})|^2$ is the cross section for excitation to the state n_l, $L_l = 1$, M_{L_l}, S_l, M_{S_l} which is independent of spin quantum numbers. It also follows (8) from azimuthal symmetry about the beam axis that $\sigma_{M_L} = \sigma_{-M_L}$. It should be emphasized that the sum in Eq. 3 contains the restriction that $L_l = L_l' = 1$. The question (9-13) of whether collision induced coherence exists between states of different L_l is not investigated in the present work since only states with $L_l = 1$ radiate to the ground state. From the form of Eq. 3 it can be seen that the intensity of linearly polarized radiation for the transition exhibits in general, sinusoidal oscillations superimposed on an exponential decay. The frequency of

the oscillations corresponds to the energy splitting of the coherent fine structure states.

Earlier beam-foil experiments (14-17) used an external electric field as a perturbation of the atomic system to produce eigenstates which are admixtures of states of opposite parity. This method also produces coherence of decaying states and provides a method of measuring Stark-perturbed-Lamb-shift splittings in excited levels of hydrogen atoms. The oscillations produced by an external electric field are called Stark quantum beats; hence, the fine structure interference effects are labeled as zero-field quantum beats to emphasize the fact that no external perturbation is applied to the system of atom plus radiation field.

The particular transition studied in the present work is from the n = 3 to the n = 1 level in hydrogen. Since only the L = 1 states of n = 3 contribute to the intensity of this transition, there are only two upper states $3p_{3/2}$ and $3p_{\frac{1}{2}}$ which decay to the $1s_{\frac{1}{2}}$ ground state with the emission of Lyman-β radiation (1026 Å). These levels are shown in Fig. 1. For this case the total intensity I, which is the sum of I_q over all polarization components q, is given by the expression

$$I = c[2\sigma_1 + \sigma_0] \exp(-\gamma t) \qquad (4)$$

where $\sigma_1 = \sigma(n=3,\ L=1,\ |M_L|=1)$ $\sigma_0 = \sigma(n=3,\ L=1,\ M_L=0)$, γ is the radiative decay constant of the n = 3, L = 1 states of hydrogen, and

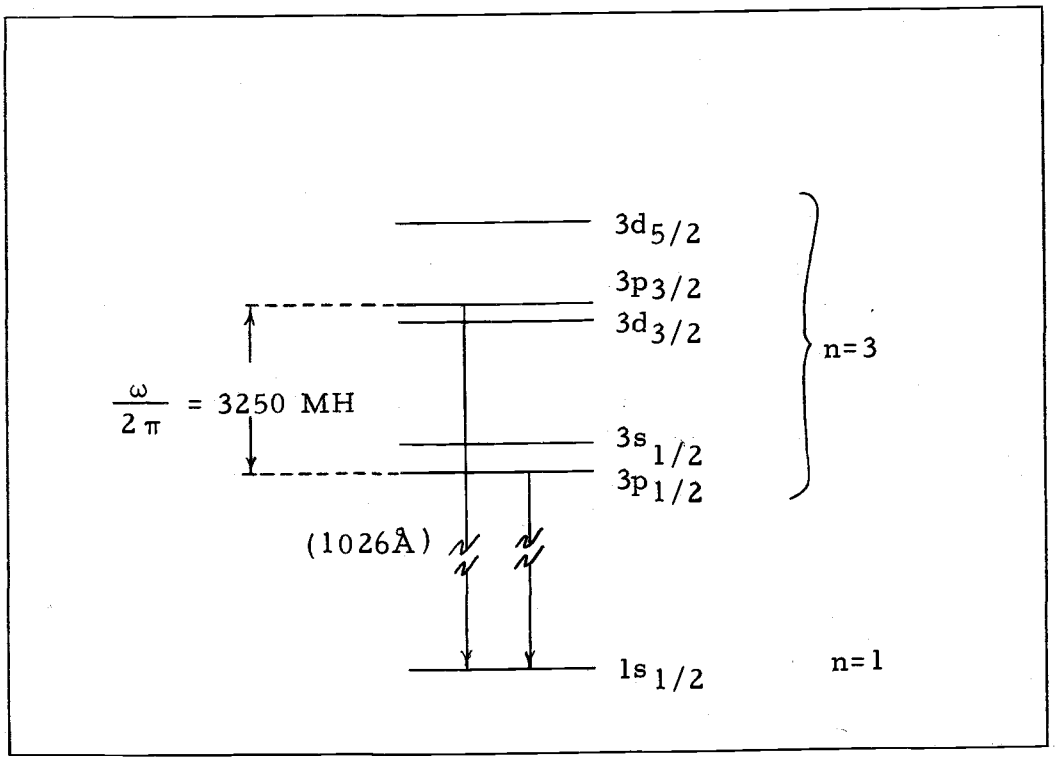

Fig. 1. Fine structure energy levels of the n=3 level of hydrogen showing transitions to the ground state.

c is a constant. The intensity of radiation with linear polarization parallel to the beam axis, I_o, is

$$I_o = \frac{4}{9} c [\sigma_1 + \frac{5}{4}\sigma_o + (\sigma_o - \sigma_1)\cos\omega t]\exp(-\gamma t) \qquad (5)$$

where $\hbar\omega$ is the energy separation of the $3p_{3/2}$ and $3p_{\frac{1}{2}}$ states. Eqs. 4 and 5 give intensities summed over all solid angle. In the present experiment, the quantities investigated are related to the intensities per unit solid angle corresponding to linear polarization parallel and perpendicular to the beam axis, observed at 90° to the beam axis.

The intensity per unit solid angle of Ly-β photons, corresponding to the radiative decay from the n = 3 level to the n = 1 level in hydrogen, with E vector perpendicular to the beam axis, observed at 90° to the beam axis is

$$I_{\perp} = \frac{3}{16\pi}(I - I_o) = \frac{c}{24\pi}[7\sigma_1 + 2\sigma_o - 2(\sigma_o - \sigma_1)\cos\omega t]\exp(-\gamma t). \qquad (6)$$

The intensity per unit solid angle of Ly-β photons with E vector parallel to the beam axis, observed at 90° to the beam axis is

$$I_{\parallel} = \frac{3}{8\pi} I_o = \frac{c}{24\pi}[4\sigma_1 + 5\sigma_o + 4(\sigma_o - \sigma_1)\cos\omega t]\exp(-\gamma t). \qquad (7)$$

Therefore, an experimental measurement of any linear combination of $I_{\parallel}$ and $I_{\perp}$ determines γ, ω, and the ratio σ_1/σ_o for the n = 3 level of hydrogen.

The sinusoidal oscillations predicted by theory may not be detectable for a given experiment. In some cases the beat frequency

of the oscillations may be so large that many beat wavelengths are integrated by the detection system, which has a finite time resolution. For the extreme opposite situation, when γ is much greater than ω, the wavelength of the oscillation is much greater than the decay length of the exponential falloff of intensity.

For the present experiment, the detection system samples a beam length which is comparable to the wavelength of a fine structure beat, but very small compared to the wavelength associated with a hyperfine frequency. Further, a measured decay length is small compared to a hyperfine beat wavelength; thus any hyperfine effects appear as corrections to the decay rate for the intensity decay curves to be discussed in Section Four (9).

Theory of Measurements

In the actual experiment neither $I_{\perp}$ nor $I_{\parallel}$ was measured directly. Fig. 2 shows a schematic diagram of the detection system used to measure intensity as a function of the position along the beam axis. The spectrometer which isolates the Lyman-β emission line transmits both $I_{\perp}$ and $I_{\parallel}$, but each with a different efficiency. Furthermore, as indicated in the previous paragraph, this instrument views a finite length of the beam rather than a single point on the beam axis. Therefore, the signal seen by a photon detector at the exit slit of the spectrometer represents a linear combination of

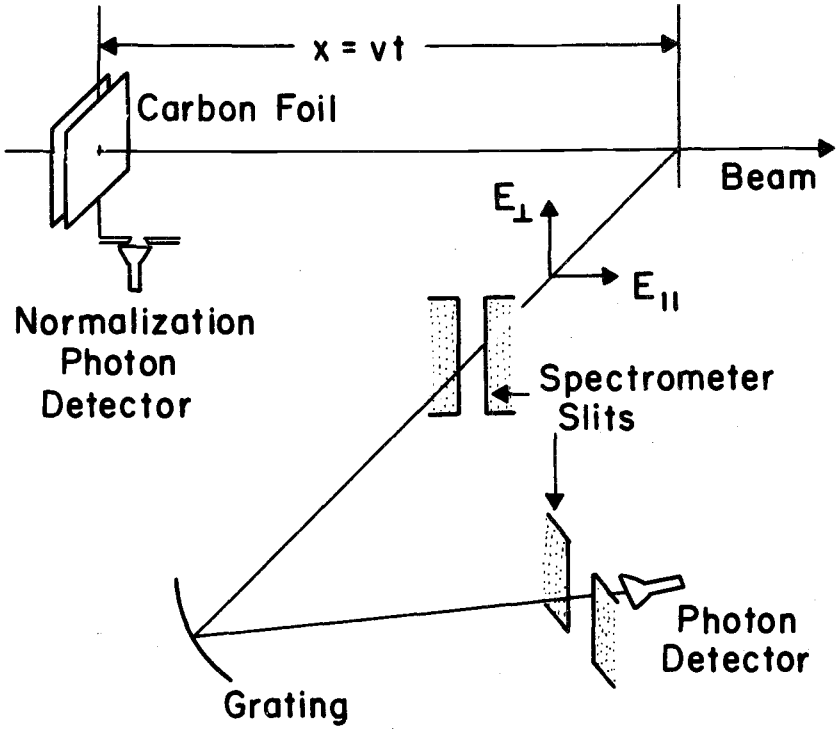

Fig. 2. Schematic diagram of the detection system used to measure intensity of radiation of the beam as a function of the position along the beam axis.

$I_\perp$ and $I_\parallel$ integrated over a time interval corresponding to the beam length viewed.

We define a spectrometer polarization parameter, g, to be the ratio of the transmission efficiency of the spectrometer for photons with E vector parallel to the slits to the transmission efficiency for photons with E vector perpendicular to the slits. The signal from a polarization insensitive photon detector at the exit slit of the spectrometer corresponding to the intensity of radiation from a single point on the beam axis is

$$s(g, \sigma_1, \sigma_o, t) \propto (I_\parallel + gI_\perp) \propto [1 + M_o(g, \sigma_1, \sigma_o)\cos\omega t]\exp(-\gamma t) \qquad (8)$$

where

$$M_o(g, \sigma_1, \sigma_o) = \frac{2(g-2)(\sigma_1 - \sigma_o)}{(4+7g)\sigma_1 + (5+2g)\sigma_o}; \qquad (9)$$

thus M_o characterizes the modulation amplitude of the non-integrated signal, $s(g, \sigma_1, \sigma_o, t)$. The theory of the determination of g is discussed in the Appendix; its measurement for the present work is detailed in Section Four.

Due to the finite angular aperture and slit width of the spectrometer, a significant fraction of a quantum beat wavelength is integrated by the signal detector. Fig. 3 defines the slit function, $f(t, t', \varepsilon, \delta, v)$, which determines how the beam is sampled by the spectrometer. In Section Four the measurement of f is discussed.

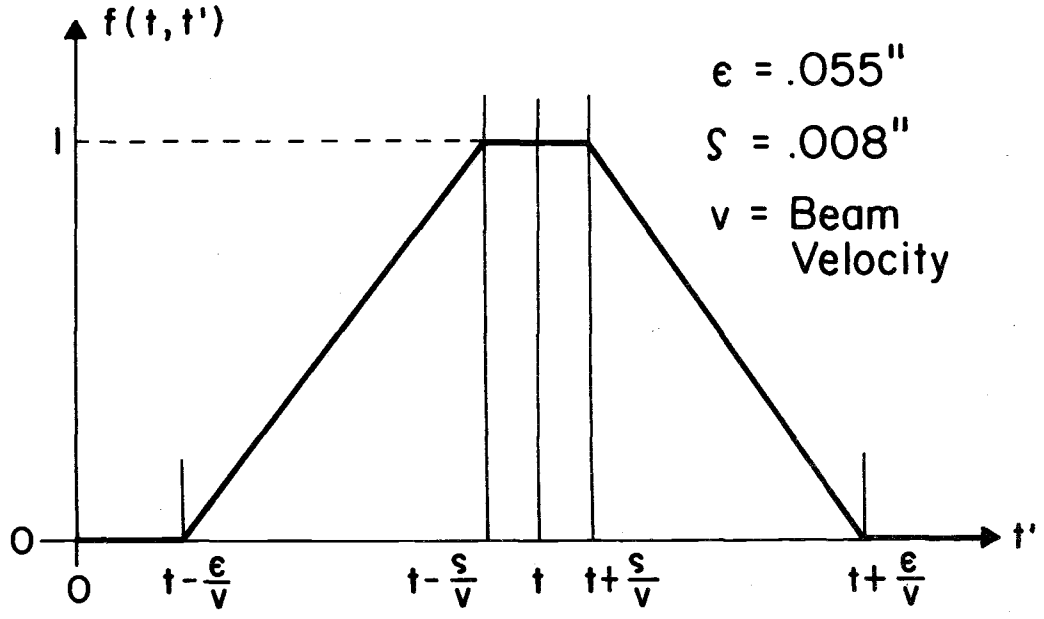

Fig. 3. Shape of the measured slit function for the signal detection system.

Now we can write the general form for the signal from a polarization insensitive detector at the exit slit of the spectrometer. This integrated signal, S, is given by the expression

$$S(t, g, \varepsilon, \delta, v, \sigma_1, \sigma_0) = \int_0^\infty s(g, \sigma_1, \sigma_0, t')\, f(t, t', \varepsilon, \delta, v)\, dt'. \quad (10)$$

In order to evaluate this integral we make use of the fact that the slit function is non-zero over a beam length which is approximately one half of a beat wavelength. Since this length is much shorter than the exponential decay length ($\gamma/\omega \simeq 1/110$), the exponential factor, $\exp(-\gamma t')$, in $s(g, \sigma_1, \sigma_0, t')$ may be expanded about the center point, t, of the slit function $f(t, t', \varepsilon, \delta, v)$ in evaluating the integral in Eq. 10. To lowest order in γ/ω, the result for the integrated signal is

$$S(t, g, \varepsilon, \delta, v, \sigma_1, \sigma_0) = \text{constant} \cdot [1+M(g, \sigma_1, \sigma_0, \varepsilon, \delta, v)\cos\omega t]\exp(-\gamma t), \quad (11)$$

where

$$M(g, \sigma_1, \sigma_0, \varepsilon, \delta, v) = \left[\frac{2(g-2)(\sigma_1-\sigma_0)}{(4+7g)\sigma_1+(5+2g)\sigma_0}\right] \cdot \left[\frac{2(\cos(\omega\delta/v)-\cos(\omega\varepsilon/v))}{\omega^2\left(\frac{\varepsilon^2}{v^2}-\frac{\delta^2}{v^2}\right)}\right]. \quad (12)$$

M is the modulation amplitude of the sinusoidal oscillations appearing in S, the integrated signal which is observed experimentally. This result is the basic equation relating the experimentally determined modulation, M, to the relative cross sections σ_1 and σ_0 for population of the magnetic substates of the L = 1 states of the n = 3 level

of hydrogen. From an inspection of Eq. 12, it is seen that the parameters g, ε, δ,ω and v also must be determined in order to extract the relative cross sections from the measured modulation amplitude.

APPARATUS

Beam Source

In order to be able to perform a beam-foil experiment with reasonable intensities of emission lines for hydrogen atoms having beam energies in the range from 200 to 500 keV, a beam current of the order of five microamps is needed on the carbon foil target. The beam source for this experiment is the four MeV Van de Graaff accelerator (High Voltage Engineering Corp. Model K) at the Nuclear Physics Laboratory of the University of Oregon. Hydrogen ions (H^+, H_2^+ and H_3^+) are extracted from a duo-plasmatron ion source at the high voltage terminal of the accelerator, and accelerated to an appropriate energy. Fig. 4 shows a schematic diagram of the ion beam path from the source to beyond the target.

When a beam of ions enters a uniform magnetic field, the radius of curvature for the trajectory is given by $r = \sqrt{2EM}/qB$, where E, M and q are the energy, mass and charge, respectively, of the ions, and B is the magnetic flux density. The field of a bending magnet can therefore be used to select the mass-energy product for a beam of ions. Since the energy of the ions is already approximately determined by the acceleration stage of the Van de Graaff, the bending magnet field strength determines both the mass

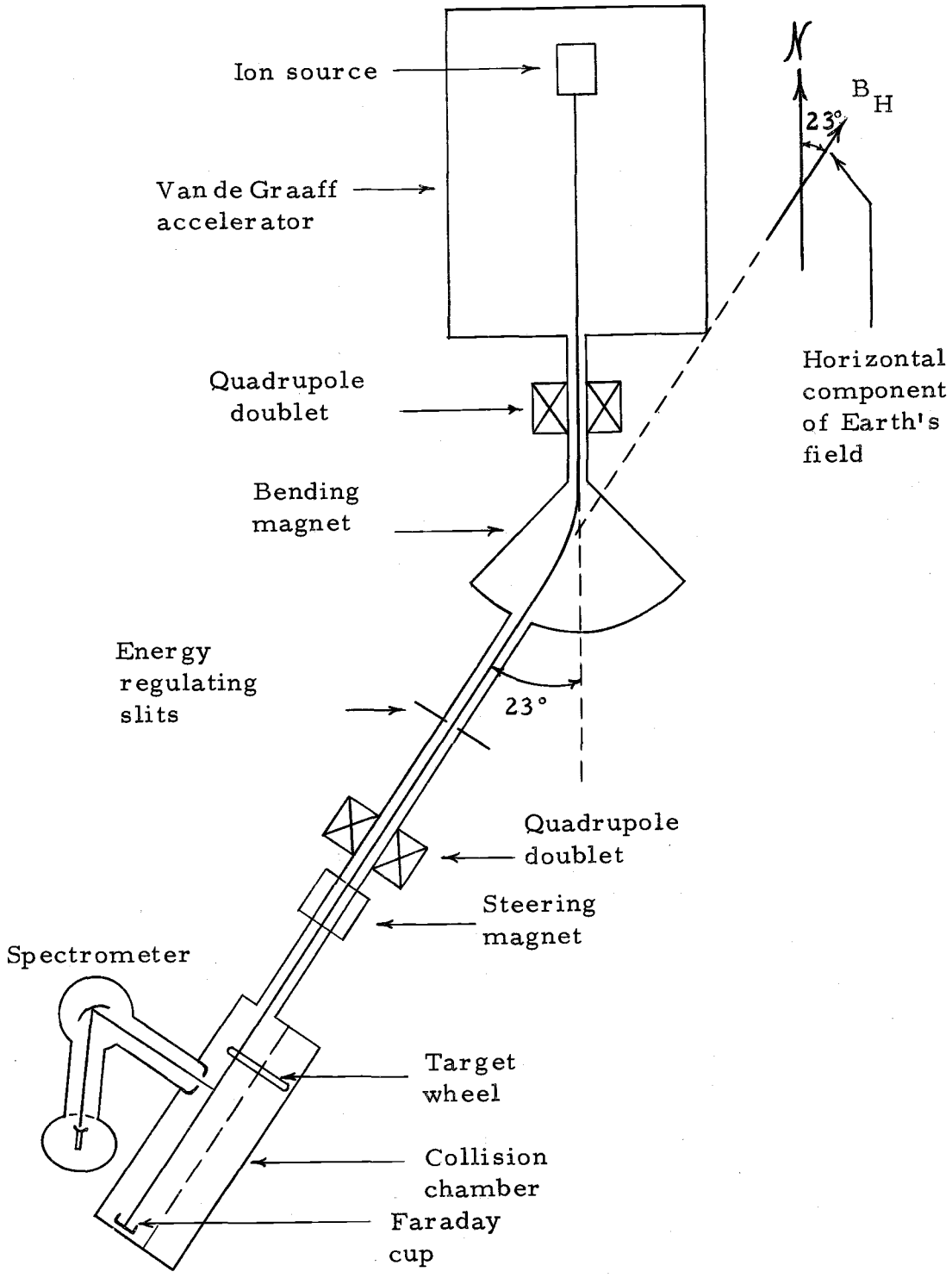

Fig. 4. Schematic diagram of apparatus showing ion beam path.

and energy for ions bent through a given angle. Once the ions with the selected energy and mass pass through the bending magnet, they travel down an evacuated beam tube toward the collision chamber.

A pair of vertical slits are located and centered on the beam tube axis approximately five feet down the beam tube from the bending magnet. Each slit blade collects ion current from one horizontal edge of the beam cross section at that point. If the beam energy changes by a small amount, more current falls on one slit and less on the other. The difference in current on these slits is used in a feedback circuit to regulate the acceleration voltage of the accelerator, serving to stabilize the beam energy. Electrostatic lenses in the ion source and magnetic lenses (quadrupole pairs) along the beam path are adjusted to focus the beam on a target in the collision chamber. With this particular accelerator, it was found that an additional steering magnet was needed along the beam tube because the beam does not emerge from the acceleration stage at the same point from one run to the next. Small corrections to the horizontal and vertical positions of the beam at the target are made with this magnet. The correction angle is always less than three milliradians, so the beam axis and the axis of the collision chamber remain parallel to within that limit (after initial alignment).

Collision Chamber

The collision chamber, shown schematically in Fig. 5, is a stainless steel cylindrical chamber which is evacuated to a base pressure of about 5×10^{-7} torr. A five inch diameter wheel, on which various targets are mounted, can be rotated about the chamber axis which is parallel to the beam axis but is offset by two inches. This target wheel may be rotated in 45° increments allowing eight different targets to be positioned on the beam axis. Independent of the rotational motion, the target wheel can be translated along the chamber axis in steps as small as .001 inch. A micrometer mechanism translates the target wheel through a rotary vacuum seal. The micrometer, which has a backlash of approximately .010 inch, is driven by a stepping motor. A Spiraltron photon detector (18) translates with the target wheel such that it always views a length of the beam at a fixed distance behind the target. The principle of operation of this detector is quite similar to that of a Channeltron detector, which is discussed in the next section. A fixed count rate in this normalization detector indicates that neither the beam nor the foil properties are varying during a run.

There are eight positions on the target wheel where various targets may be mounted. One of the eight targets is a quartz disk. Since quartz fluoresces where it is struck by the ion beam, this disk gives

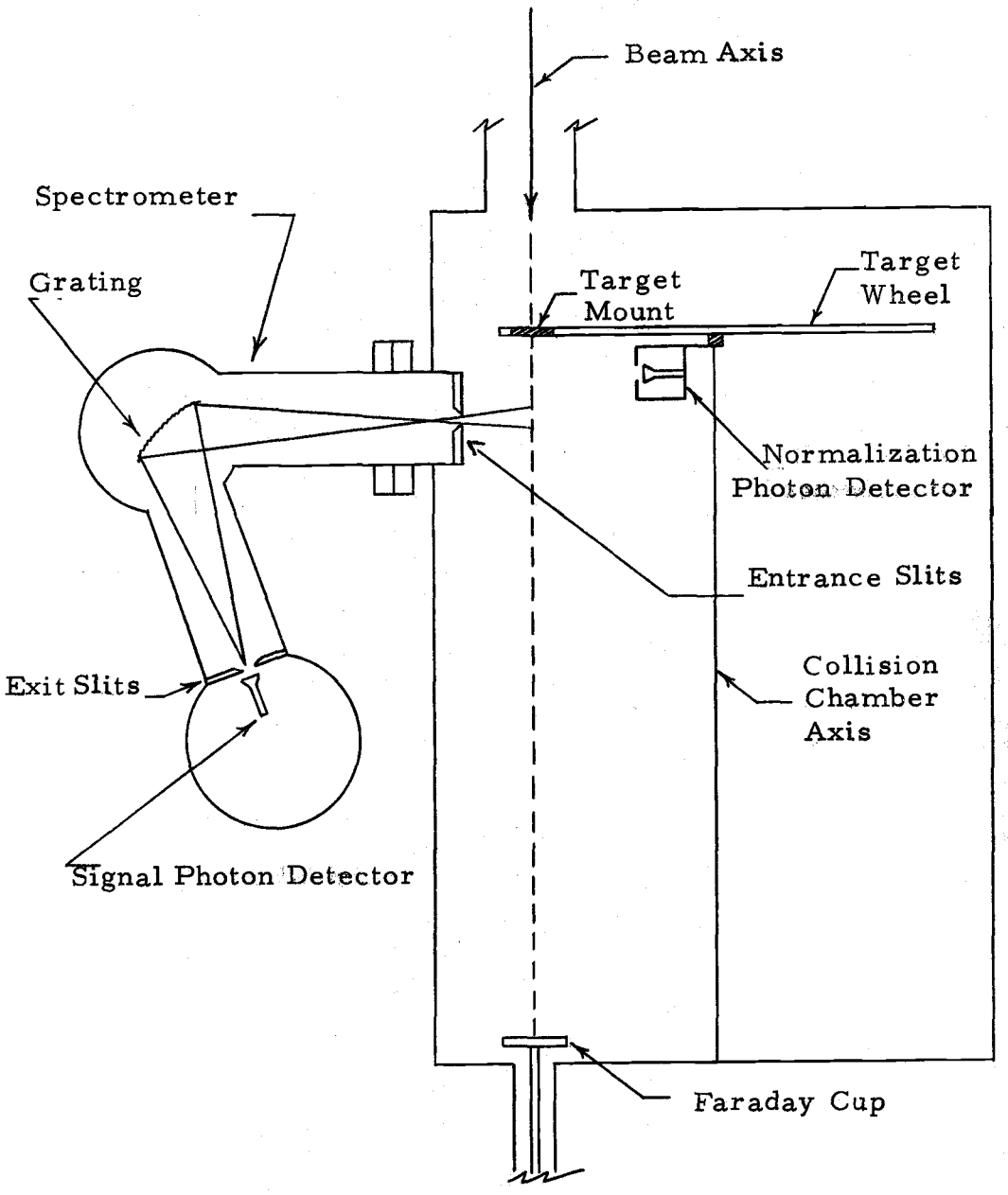

Fig. 5. Collision chamber and spectrometer.

a visual indication of the beam size and position. The carbon foil targets are supported by thin tantalum target holders having a 1/4 inch hole which the foil covers. Whenever the ion beam is H_2^+ or H_3^+, two carbon foils are inserted in the beam path. The purpose of the first foil is to dissociate the molecular ions; whereas the second foil defines t = 0 for the excitation of the hydrogen atoms (15). In the present experiment, which uses H_2^+ or H_3^+ ions, the two carbon foils are separated by a distance of approximately .2 inch.

The carbon foil targets, obtained from the Yissum Research Development Co., Jerusalem, are 10 $\mu g/cm^2$ thick. The foil is originally made by sputtering carbon onto a thin sheet of glass. In order to mount the foil on a target holder, it must first be removed from the glass by dipping the glass into water, causing the foil to float to the surface. A drop of household detergent added to the water lowers its surface tension. The foil can then be mounted by slipping a target holder under the foil and carefully lifting the assembly out of the water with the foil and target holder in a vertical plane.

In addition to several carbon foil targets and the quartz target, one empty tantalum target holder is mounted on the target wheel. There is also one position on the target wheel where no target or holder of any kind is mounted, which may be rotated onto the beam axis. These last two arrangements allow the beam to reach a Faraday cup at the back end of the collision chamber without any targets being

in the path.

For the present work, the Faraday cup is simply a two inch copper disk, centered on the beam axis, which collects the beam current. It is usually biased positively with respect to ground to reduce emission of secondary electrons produced at its surface by the incident beam. The current from the Faraday cup, while not exactly the true positive ion beam current (because of electrons stripped from the foil and carried in the beam (3) and secondary electron emission at the Faraday cup itself), is proportional to the beam current. Since the number of atoms per unit length of the beam downstream from the foil is proportional to the Faraday cup current, the intensity of Lyman-β radiation measured by the spectrometer is also proportional to this current.

Signal Detection System

As shown in Fig. 5, the spectrometer assembly is mounted on a flange of the collision chamber such that it views a section of the beam at approximately 90° to the beam axis. The spectrometer is a .5 meter Seya-Namioka type (19) with a McPherson Co. gold replica grating of 1200 lines per millimeter, blazed for 1500 Å. The unit, which was locally designed and constructed, has a linear reciprocal dispersion of 16.6 Å/mm. An external drive allows the grating to be rotated with the unit under vacuum to investigate

radiation from the visible to the extreme ultraviolet region of the electromagnetic spectrum. As used in the present experiment, the grating is positioned such that Lyman-β radiation (1026 Å) passes through the exit slits. The entrance and exit slit spacings were .045 inch and .050 inch, respectively. At the exit slit a Bendix Channeltron photon detector, model 4028, counts Lyman-β photons.

A Channeltron detector (20) is basically a hollow helix attached on one end to a small cone which serves as a photocathode. This entire device is made from a lead glass material which has a work function similar to that of Tungsten (4.5 eV). Fig. 6 shows a diagram of the detector and the circuitry used in conjunction with it. When photons with wavelengths less than 1500 Å strike the photocathode, electrons are emitted from this surface. The quantum efficiency (output electrons per photon incident on the photocathode) is 6% at 1026 Å (21). An electric field, produced by the potential difference applied across the entire length of the Channeltron, which has a resistance of about $10^9 \Omega$, accelerates these electrons down the inside of the helix. Each time electrons strike the inner wall of the helix, secondary electrons are emitted, producing electron multiplication. A short (nominally forty nanosecond) pulse of electrons is the output at the positive voltage end of the helix caused by an initial photoelectron at the cathode. A nearby anode is biased to collect this electron pulse, which is typically of the order 10

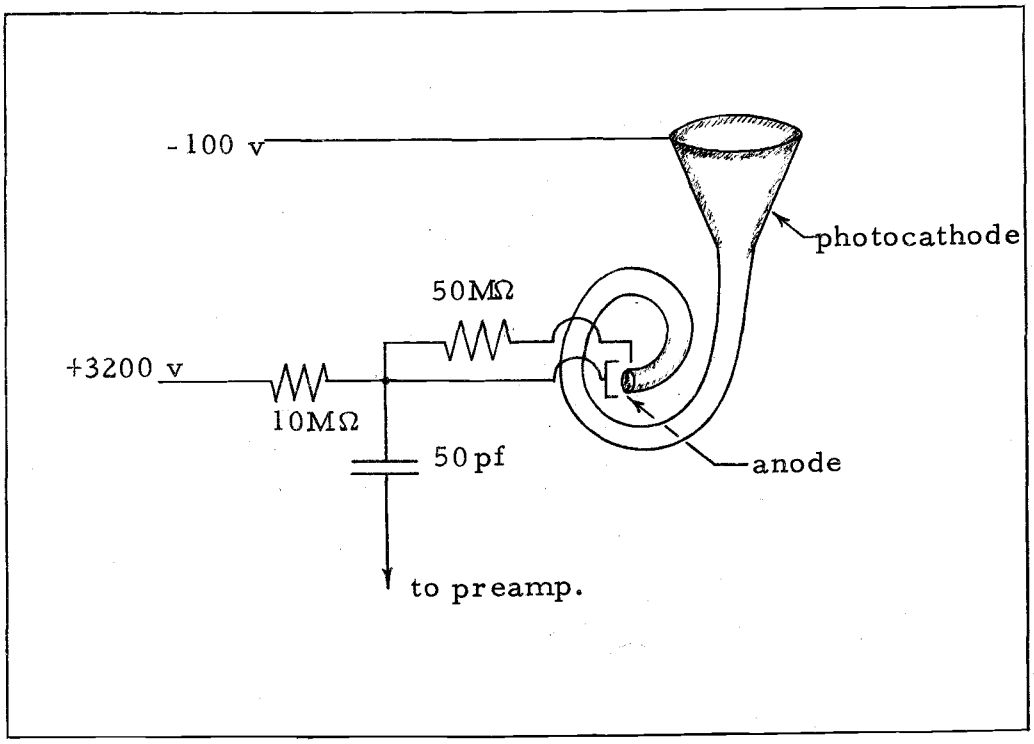

Fig. 6. Channeltron photondetector circuit.

picocoulombs. This charge pulse, in turn, is converted into a voltage signal by a charge sensitive preamplifier. The voltage pulse out of the preamp is amplified and counted using standard pulse counting circuitry discussed below. The electron gain of the Channeltron is nominally 10^8. Its pulse height distribution is approximately Gaussian with a full width at half maximum of fifty percent at this gain.

Since a Channeltron detects electrons incident on the cathode with approximately 100% quantum efficiency and Lyman-β photons with 6% quantum efficiency, it is necessary to bias the cathode 100 volts negative with respect to ground. This bias prevents low energy electrons from reaching the photocathode. These low energy electrons are produced by the ultraviolet radiation incident on various surfaces in the spectrometer (19).

Two important advantages of a Channeltron detector over other photon detectors for extreme ultraviolet radiation, are its narrow pulse height distribution and its low dark current (output pulses with no signal radiation incident on the photocathode) which is less than five counts per minute (18). Because the dark current count rate is so small, there is negligible background due to the detector in signal count rate data.

Electronics

There are four quantities which are recorded during a data run at a given position of the foil along the beam axis: the integrated beam current, the signal counts from the Channeltron detector at the exit slit of the spectrometer, the counts from the Spiraltron detector which moves with the foil, and the real time interval for counting. The last three quantities are normalized to a fixed value of the first. Fig. 7 shows a block diagram of the circuitry used for data acquisition.

The output from each of the photon detectors is a charge pulse which is converted to a voltage pulse by Hewitt Packard Model 5554A charge sensitive preamplifier. This voltage pulse is amplified by a linear voltage amplifier (Tennelec model TC 213) and the amplified voltage pulse is fed through a discriminator. The discriminator gives a logic pulse output if the input voltage pulse is greater than the fixed discrimination voltage of the unit. A slave scalar counts and displays the discriminator output pulses.

The current from the Faraday cup is fed into a current integrator-digitizer (Ortec model 439). The count rate of logic pulses out of the integrator-digitizer is proportional to the current input. These logic pulses are counted and displayed in a master scalar. A pulser (Tennelec model TC 812) which outputs 60 counts per second acts as a real time clock; its voltage pulses are also

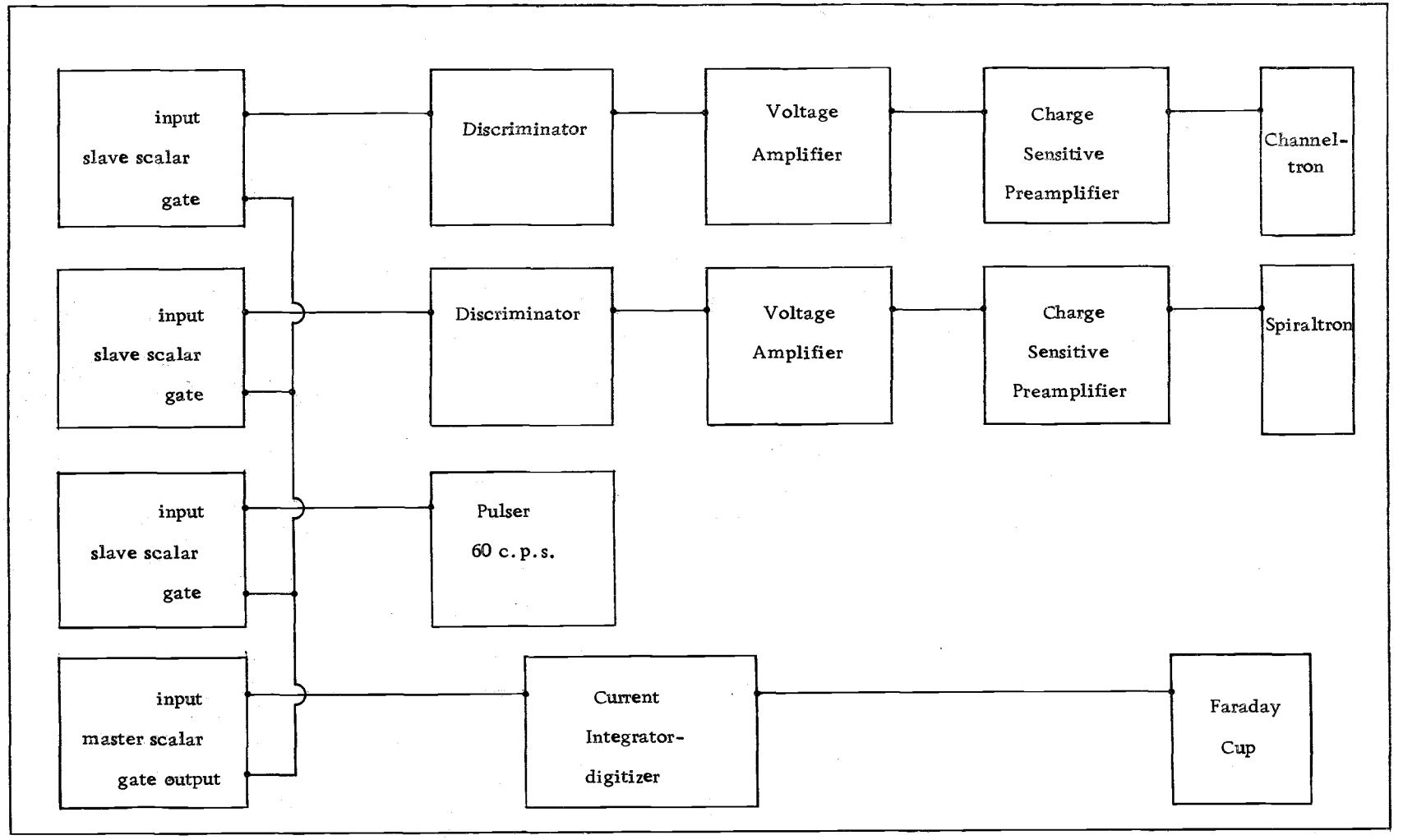

Figure 7. Pulse counting circuitry used for data acquisition.

counted and displayed in a slave scalar. When the total counts in the master scalar reach a preset value, the scalar outputs a voltage level which closes the gate at the input for each of the slave scalars.

The gate closing level change from the master scalar also generates a pulse in a logic circuit which controls the stepping motor used to advance the target wheel. The logic circuit is designed such that the target wheel can be translated a preset distance each time the master scalar gates the other scalars off. Thus, the foil is automatically advanced to the next data taking position at the end of each data acquisition interval. A manual switch controls the reopening of the scalar gates to begin the next data acquisition.

Magnetic Field

It is necessary to cancel the earth's magnetic field in a zero-field experiment because any magnetic field component perpendicular to the beam axis produces a motional electric field, $\vec{E} = \vec{v}/c \times \vec{B}$. Magnetic fields on the order of one gauss can give rise to appreciable Stark mixing of both s and d states with the p states in the n = 3 level of hydrogen (13). For example, a 500 keV beam of hydrogen atoms moving through a magnetic field of one gauss experiences an electric field of 10 volts/cm. This electric field mixes the $3s_{\frac{1}{2}}$ and $3p_{\frac{1}{2}}$ states of the hydrogen atoms such that the probability amplitude of the perturbed p state contains a 16% mixture of the $3s_{\frac{1}{2}}$ state (23).

The angle of declination of the earth's magnetic field in the vicinity of the collision chamber is 23° east of geographic north, and its angle of inclination is 70° below horizontal. The beam tube and collision chamber axes are also 23° east of north, therefore, only the vertical component of the earth's magnetic field is perpendicular to the path of the foil-excited hydrogen atoms. This component has a magnitude of approximately .5 gauss.

Ideally, a Helmholtz pair of coils (24) could be situated about a vertical axis such that the magnetic field produced by the pair exactly cancels the vertical component of the earth's field along the beam axis between the target wheel and the spectrometer. In practice, it is not possible, physically, to position a large coil beneath the collision chamber to achieve the above situation. It was found, however, that one circular coil, 36 inches in diameter, in a horizontal plane 12 inches above the beam axis and centered about an axis which intersects the beam axis, cancels the earth's field in the region of interest. Specifically, the net magnetic field perpendicular to the beam axis is less than .03 gauss along the beam axis from two inches upstream to one inch downstream from the spectrometer field of view when the current through the 280 turns in the coil is .16 amps.

EXPERIMENTAL METHOD AND RESULTS

Data Runs

The first step in any beam-foil experiment is to obtain in the collision chamber an ion beam of the desired energy, physical size and intensity. Pages 20 to 22 of Section Three describe the path of a beam from the ion source to the collision chamber. In the chamber, the beam size and position are determined visually by inserting a quartz disk target into the beam path, since quartz fluoresces when struck by the beam. Final beam focus is achieved by minimizing the beam spot size on the quartz and maximizing the Faraday cup current with no target in the beam path. Typically, the beam is a 0.25 inch diameter spot on the quartz. The Faraday cup current is usually three to six microamperes. It should be mentioned that the ion beam dimensions do not vary appreciably along the beam axis over several inches. During an actual data run the foil traverses a distance of about one inch along the beam axis.

Having obtained a good beam, a preliminary data scan is then taken. There are four quantities which are recorded at a given position of the foil along the beam axis: the integrated beam current, the signal counts from the Channeltron detector at the exit slit of the spectrometer, the counts from the normalization Spiraltron

photon detector, and the real time interval for counting. The last three quantities are normalized to a fixed value of the first. With this method of normalization any fluctuations in beam intensity do not affect the counts from the signal detector. The counts from the normalization detector (Spiraltron) remain constant if foil properties do not change. The real time measurement serves as a check on long term stability of the beam. A preliminary data scan amounts to recording the four above mentioned quantities for values of x from -.5 inches to 2.0 inches at .1 inch intervals. This provides a quick check on the beam and the experimental apparatus by tracing out roughly the exponential decay of the 3p states of hydrogen. Another consistency check used is to repeat this scan with the spectrometer adjusted to pass Lyman-α radiation (1216 Å) and to trace out the exponential decay of the 2p states.

After completing the preliminary data scan, the actual data run is begun. Data are taken over a range of x of approximately one inch, beginning at x = .2 inch and advancing, usually, in increments of .02 inch. Data are taken at each position for a real time interval of one to five minutes, depending on the signal count rate. After a preset count is recorded for the integrated Faraday cup current, the foil (i.e. target wheel) is advanced automatically to the next position. Data are displayed on scalars but, presently, are recorded by hand. A single data scan consists of the data recorded

for the 50 or so values of x, spaced .02 inches apart in the range 0.2 in. $\lesssim x \lesssim$ 1.2 in. A complete data run for a particular beam energy is obtained by repeatedly scanning x over this range until the statistical uncertainty in signal detector counts is considerably less than the amplitude of the modulation appearing in the signal decay curve. In Figs. 8, 9, 10 and 11, completed data runs are shown for various energies of the foil-excited hydrogen atoms ranging from 230 to 490 keV. Data were not taken closer to the foil because of a large background near the foil. It is seen by inspection that the decay curves just described are approximately of the form of a modulated decaying exponential function, with a modulation frequency approximately equal to the fine structure splitting of the 3p levels of hydrogen (3, 250 MHz) and a decay constant approximately equal to the reciprocal of the natural lifetime of these levels (5.4 nsec.). In order to further analyze these data, in terms of the theory developed in Section Two, it is necessary to know the spectrometer polarization parameter, g, the slit function, f, and the absolute position of the foil.

Measurement of the Intrinsic Polarization of the Spectrometer

The theory involved in the determination of the spectrometer polarization parameter is developed in an appendix. The basic result of that discussion is (23)

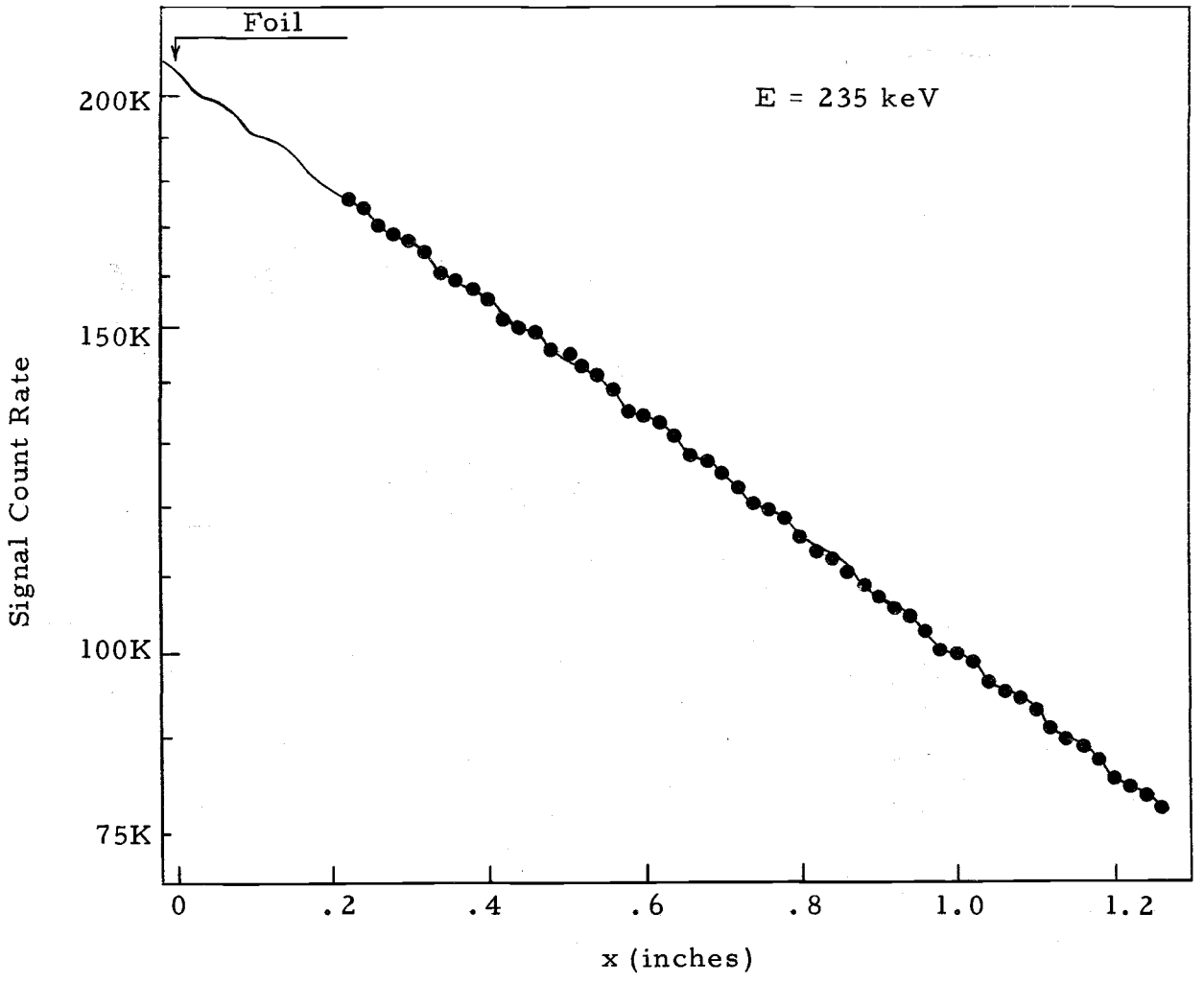

Fig. 8. Normalized signal count rate as a function of the distance from the foil to the spectrometer field of view. 235 keV beam energy per atom.

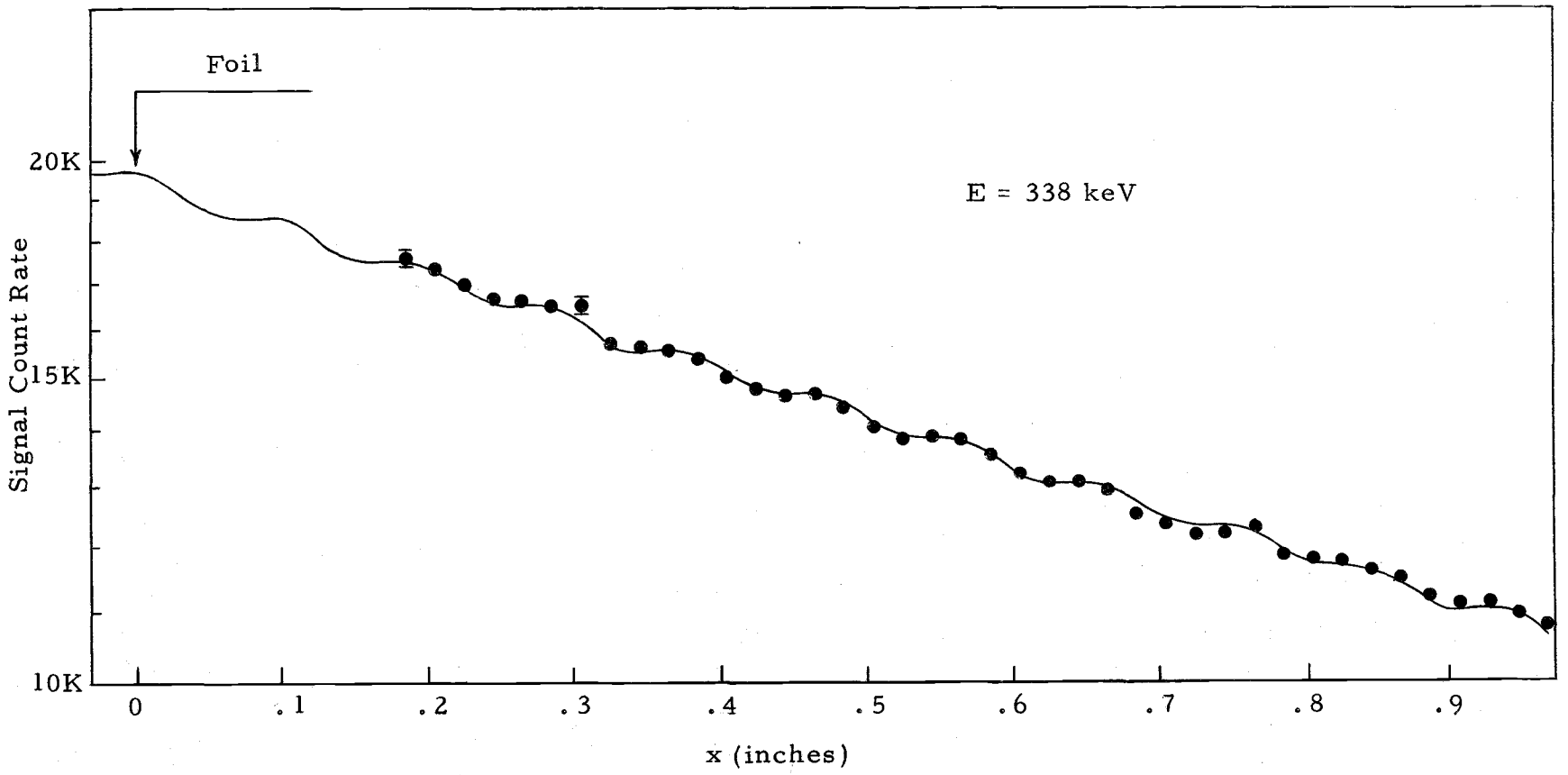

Fig. 9. Normalized signal count rate as a function of the distance from the foil to the spectrometer field of view. 338 keV beam energy per atom.

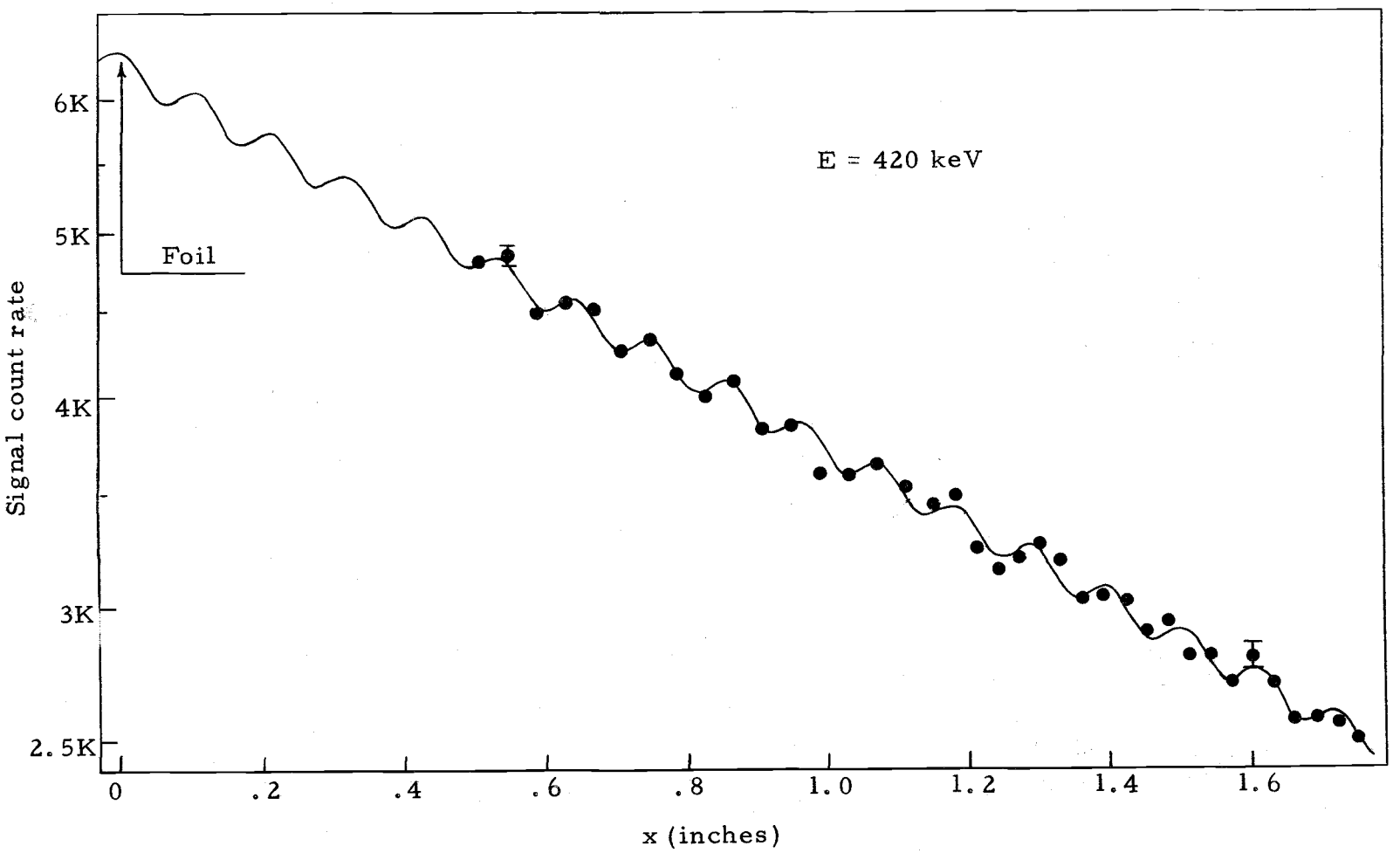

Fig. 10. Normalized signal count rate as a function of the distance from the foil to the spectrometer field of view. 420 keV beam energy per atom.

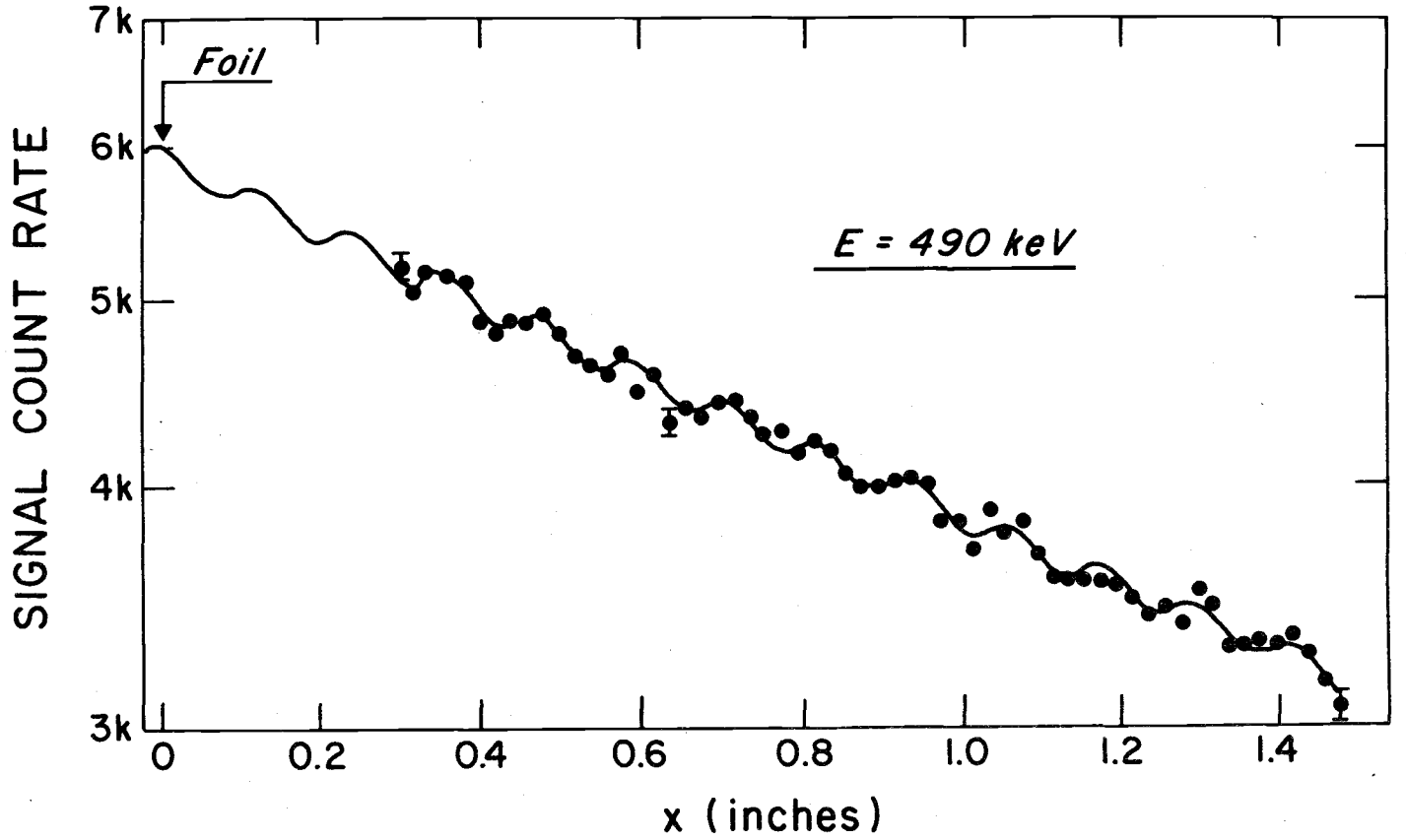

Fig. 11. Normalized signal count rate as a function of the distance from the foil to the spectrometer field of view. 420 keV beam energy per atom.

$$g = \frac{R_2[1+4(R_1+R_2)]^{\frac{1}{2}} - (R_2+2R_1)}{R_1[1+4(R_1+R_2)]^{\frac{1}{2}} - (R_1+2R_2)} \qquad (13)$$

where R_1 is the net 45° reflectance from an opaque, homogeneous and non-magnetic material with the reflecting surface oriented so that the plane of incidence is perpendicular to the exit slit of the spectrometer, and R_2 is the net reflectance when the plane of incidence is parallel to the exit slit. In this section the determination of R_1 and R_2 is discussed for two different reflecting materials, polished quartz and common microscope slide glass (Borosilicate). This measurement was performed when the spectrometer was mounted to a small vacuum chamber which contained an unpolarized ultraviolet light source.

Fig. 12 shows a schematic diagram of a portion of the apparatus used to determine R_1 and R_2 for Lyman-β radiation. Not shown is an ionization type pressure gauge which is the source of unpolarized radiation. This source is mounted at the entrance slit of the spectrometer. The entire spectrometer chamber is evacuated to a base pressure of 5×10^{-6} torr when the reflectivity measurements are made. It should be noted in Fig. 12 that a thin sheet of brass, having a pin hole (.050 in. diameter) centered on the slit aperture, covers the exit slit. This serves to define an axis for the light beam from the center of the grating to the center of the pin hole. Initial alignment of the setup is accomplished by using a light source in the

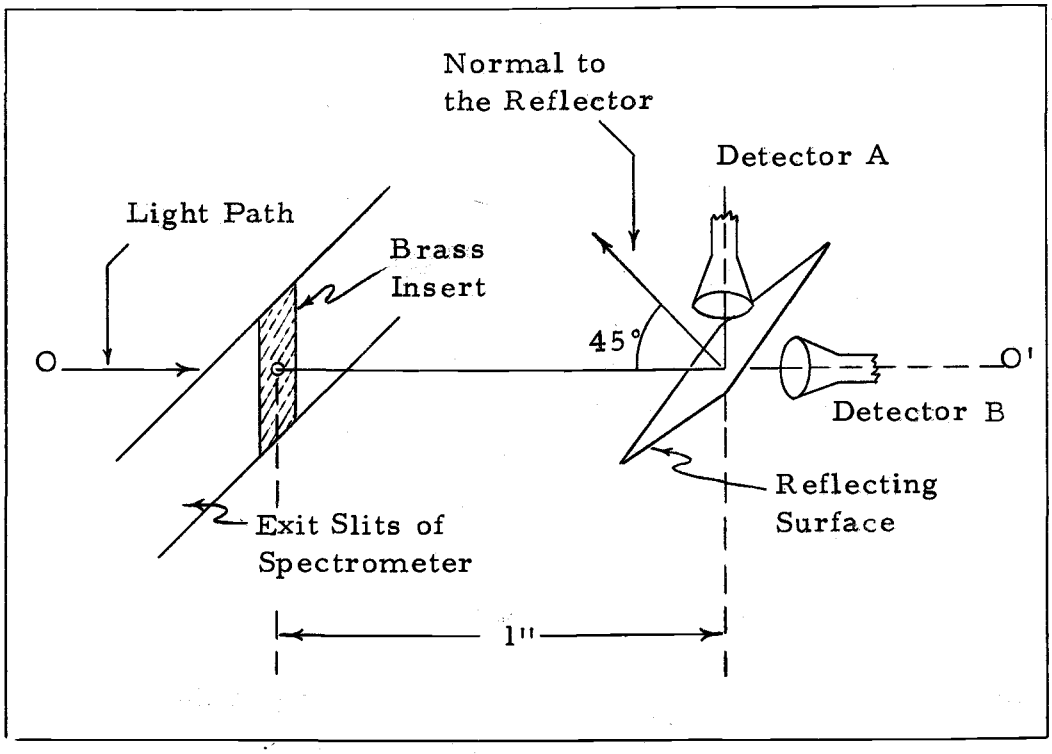

Fig. 12. The experimental setup used in measuring R_1 and R_2. Detector A and the reflecting mirror can rotate as a unit about the axis 0-0' to measure the ratio R_1/R_2. The reflecting surface can also be removed from the light path so that the absolute value of R_2 can be determined by comparing count rates in A and B.

visible region of the spectrum with the spectrometer set for zero order reflection. Two separate experiments must be performed with this apparatus to determine R_1 and R_2 for 1026 Å radiation.

In the first experiment the ratio R_2/R_1 is determined. Detector A and the reflecting surface can be rotated as a unit about the axis 0-0' in Fig. 12. The ratio of the measured count rate from detector A when the plane of incidence is parallel to the original exit slit to the measured count rate from A when the plane of incidence is perpendicular to the exit slit gives R_2/R_1 directly. The pulse counting circuitry used for these measurements is similar to that discussed in Section Three with the following changes: signal counts from detector A are normalized to a fixed counting time, thus directly measuring relative intensity, and the signal pulses out of the discriminator, in addition to being stored in a scalar, are also fed into a pulse ratemeter (Tennelec model TC 590) which gives a voltage level output proportional to the count rate input. This voltage level is plotted versus time on a (Hewitt-Packard model 7004F) X - Y recorder to verify that the light source intensity is constant while data is being taken with detector-mirror assembly in any fixed position.

Another use made of the ratemeter-plotter assembly is to verify experimentally the assumption discussed in the appendix that the linear polarization is parallel or perpendicular to the grating

rulings and slit axes. A one-turn rheostat is coupled to the rotating detector-assembly. By using the rheostat terminals as a voltage dividing circuit, a voltage level proportional to the angle of rotation of the mirror about the axis 0 - 0' is obtained. When this voltage level is used as the X - axis signal and the ratemeter voltage as the Y - axis signal, relative reflected intensity of radiation is plotted as a function of the angle of rotation. If the assumption discussed above is correct, then maxima or minima of relative intensity should occur when the plane of incidence is either parallel or perpendicular to the axis of the grating ruling. Experimentally, this is found to be the case.

The second experiment involves measuring R_2 directly. This is accomplished by measuring the signal count rate from detector A with the reflector in place as shown in Fig. 12 and then removing the reflector and measuring the signal count rate from detector B. These measurements must, of course, be done with a steady light source. The ratio of the count rate from detector A to the count rate from detector B (with the mirror removed) for the configuration in Fig. 12 is defined to be r_{2AB}. It is equal to R_2 if the detectors A and B have the same quantum efficiency. To account for any difference in the quantum efficiencies, the detectors are interchanged and the measurement is repeated. The ratio of the count rate from detector B, which now measures reflected intensity, to

the count rate from detector A, now viewing non-reflected light when the mirror is removed, is defined to be $r_{2BA'}$. It is easy to show that $R_2 = \sqrt{r_{2AB'} \cdot r_{2BA'}}$. Once R_2 is known, R_1 is calculated using the result of the first experiment which measures the ratio R_2/R_1.

Having made all of the above measurements using the polished quartz as a reflector, the entire sequence is repeated with the microscope slide glass as the reflector. The results of these measurements are summarized in Table 1. The resulting value of g is 3.4 ± 0.3.

Table 1. Summary of intrinsic polarization results.

reflector	R_1	R_2	g
quartz	$.201 \pm .007$	$.104 \pm .006$	$3.2 \pm .25$
glass	$.183 \pm .008$	$.085 \pm .006$	$3.6 \pm .25$

Measurement of Slit Function

In order to relate the measured modulation to the relative cross sections for excitation of orbital angular momentum magnetic substates, it is necessary to know the slit function $f(t, t', \varepsilon, \delta)$ which is defined above in Section One. This section describes the determination of the slit function corresponding to the configuration of the

signal detection system used in the present experiment.

The apparatus used to determine the slit function is shown schematically in Fig. 13. The point on the beam axis at the center of the field of view of the spectrometer is defined to be x. All points x' on the beam axis for which $|x-x'| < \delta$ are "seen" by all points of the grating and therefore contribute equally to the integrated signal. Points x' in the range $\delta \leq |x-x'| \leq \varepsilon$ are visible to only a fraction of the total grating surface, and therefore contribute to the total signal proportionately.

The slit function was experimentally determined by the following method. A helium-neon laser was mounted on a linear micrometer drive which translated parallel to the line representing the beam axis, with the laser axis perpendicular to the beam axis as shown in Fig. 13. A lens focused the laser light on the beam axis line. The focused laser light completely filled the entrance slit of the spectrometer when the focus point was at x on the beam axis. The focus point thus represented a point light source on the beam axis as seen by a detector at the exit slit of the spectrometer. The slit function was therefore measured directly by plotting the signal from the calibrated light detector versus the position, x', of the focus point along the line representing the beam axis. This curve is shown in Fig. 14. The detector was a vacuum photodiode (R. C. A. model 922). It was calibrated to determine that the voltage output varied

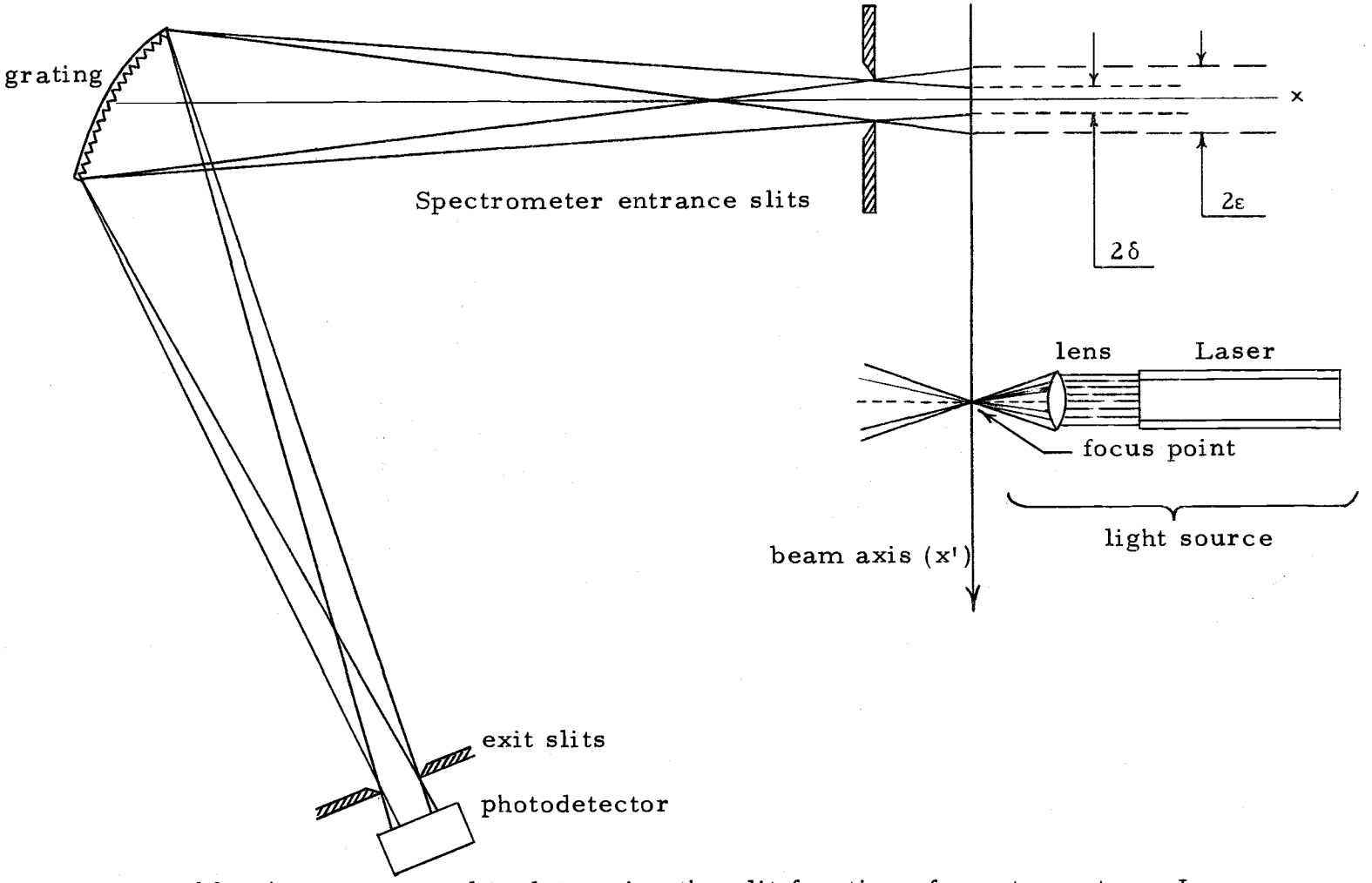

Fig. 13. Apparatus used to determine the slit function of spectrometer. Laser assembly translates parallel to line representing beam axis.

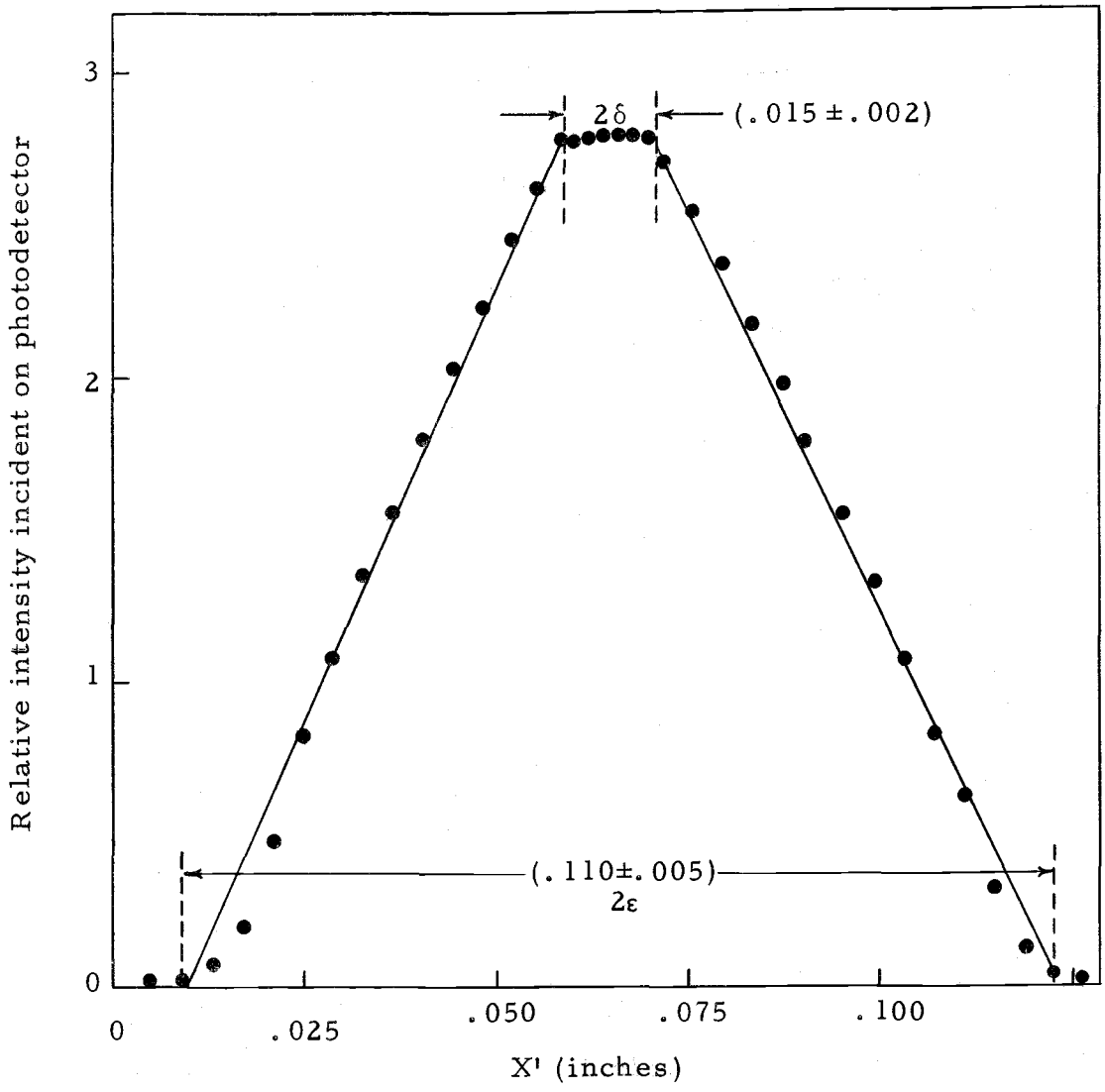

Fig. 14. Intensity at photodetector vs. relative position of source along line representing beam axis.

linearly with incident intensity on the photocathode.

It should be noted that this entire development assumes that the slit function is independent of wavelength since the results of a measurement in the visible region of the spectrum are applied to data reduction of intensity measurements in the extreme ultraviolet range. The slit function was also calculated (26) from the known spectrometer parameters to verify the experimental results given in Fig. 14.

Measurement of the Absolute Position of the Foil Corresponding to t = 0

In a separate experiment the absolute position of the carbon foil target corresponding to t = 0 for the beam-foil excitation was determined. In this experiment the detector at the exit slit of the spectrometer in Fig. 13 was replaced by the laser-lens system described above such that the focus point of the laser light was at the exit slit and the light from this source completely filled the grating surface. The grating was set for zero-order reflection so that light reflected from the grating passed through the entrance slit of the spectrometer and was incident on the line representing the beam axis in Fig. 13. The position x, which corresponds to t = 0, was then determined by visually centering the back edge of a foil holder on the illuminated section of the beam axis line. This was accomplished by visually determining the end points of the illuminated section in repeated

measurements. The point x corresponding to t = 0 was determined to be 8.266 ± .010 inches from the extreme forward position of the target wheel along the beam axis, which is a fixed position in the collision chamber.

Because data were not taken close to the foil, it was not possible to determine the t = 0 position from the signal decay data itself. Hence, the measurement just described was essential to data reduction. The importance of this measurement stems from the fact that the interference term appearing in the theoretical expression for the signal in the present experiment is proportional to $(\sigma_1 - \sigma_o)\cos\omega t$. Unless the uncertainty in ωt is less than π, it is not certain whether $\sigma_1 < \sigma_o$ or $\sigma_1 > \sigma_o$. This uncertainty allows for two solutions for the relative cross sections, σ_1 and σ_o, for a given modulation amplitude. The .01 inch uncertainty in the position of the foil at t = 0 yields an uncertainty in t which is always less than $\pi/4$, so the accuracy of the measurement of x described above is better than that needed for data reduction.

ANALYSIS

The four sets of data shown in Figs. 8-11 were each fitted to a curve of the form

$$F = \{c_1 + c_4 \cos[c_5(x-c_6)]\} \exp(-c_2 x) + c_3 \qquad (14)$$

using the method of least squares fitting (27). In Eq. 14, x is the distance along the beam axis from the foil to the center of the field of view of the spectrometer. Comparing Eq. 14 with Eq. 11, one sees that $c_4/c_1 = M$, the modulation amplitude of the beats; $c_5 = \omega/v$; $c_2 = \gamma/v$; and c_6 is the position of the foil at $t = x = 0$, where v is the beam velocity. Cascade contributions are accounted for by the constant background term c_3, since they give rise to a slowly decaying exponential which can be replaced by a constant for the distance scale used here (28).

The method of least squares fitting is predicated on the hypothesis that the optimum description of a set of data is that one which minimizes the weighted sum of squares of deviation of the data y_i from the fitting function $F(x_i)$. Thus, a measure of the goodness of fit can be defined as

$$\chi^2 = \sum_i \left\{\frac{1}{\sigma_i^2} (y_i - F(x_i))^2\right\} \qquad (15)$$

where the σ_i's are the uncertainties in the data points y_i. According to the method of least squares, the optimum values of the parameters

c_j in Eq. 14 are obtained by minimizing χ^2 with respect to each of the parameters simultaneously.

$$\frac{\partial \chi^2}{\partial c_j} = \frac{\partial}{\partial c_j} \left\{ \sum_i \frac{1}{\sigma_i^2} (y_i - F(x_i))^2 \right\} = 0 \qquad (16)$$

It is not convenient to derive an analytical expression for calculating the parameters c_j because $F(x_i)$ is a nonlinear function of the parameters. Instead, χ^2 is considered a continuous function of the parameters c_j describing a hypersurface in six dimensional parameter space, and the space must be searched for the appropriate minimum value of χ^2. Two different computer programs were used to minimize χ^2 for each set of data (27). These programs differ in the methods used to search parameter space. The use of the two independent computational methods provides a check on the correctness of the curve fitting results.

It is necessary to make initial estimates of the parameters c_j for the curve fitting programs. Since both ω and γ are known for the $n = 3$, $L = 1$ states of hydrogen, initial estimates of c_2 and c_5 can be made using the beam energy determined with a calibrated generating voltmeter, which measures the accelerating voltage of the Van de Graaff. An initial value of c_6 is provided by the measurement of the $t = 0$ foil position as discussed in Section Four. Estimates of c_1, c_3 and c_4 can be made by inspection of the raw data.

The standard fitting procedure applied to each set of data was to first fix the amplitude $c_4 = 0$ so that the parameters c_1, c_2 and c_3 could be approximately determined. Using these improved estimates of c_1, c_2 and c_3 along with the initial estimates of c_4, c_5 and c_6 (c_4 no longer zero), a reasonable fit was usually obtained by allowing all parameters to vary independently. For the final fitting the ratio of c_5/c_2 (i.e. ω/γ) was fixed to be 109.8, thus reducing by one the number of independent parameters. The results of the fitting calculations are shown in Table 2. The errors quoted represent an uncertainty of one standard deviation in the parameters.

The quantity in Table 2 which indicates the goodness of the fit in each case is χ^2_ν, the reduced chi-square, which is defined in the following equation:

$$\chi^2_\nu = \frac{\chi^2}{\nu} \tag{17}$$

where $\nu = N-6$, N being the number of data points fitted. As long as χ^2_ν is reasonably close to one, that is less than 1.5, the probability is greater than .5 that the fitting function is correct (25).

The values of the parameters c_j in Table 2 can be used to calculate several quantities of physical interest. The fine structure splitting of the L = 1 states in the n = 3 level of hydrogen is given (in frequency units) by

$$\Delta E = \frac{1}{2\pi} c_5 \nu \tag{18}$$

Table 2. Results of curvefitting.

Run	Energy (keV)	c_1	c_3	c_4	c_5 ($inch^{-1}$)	c_6 (inch)	χ^2_ν
1	235. ± 10.	178,590. ± 2,380.	-9,814. ± 2,450.	596. ± 91.	80.1 ± .7	-.008 ±.008	1.9
2	338. ± 10.	16,684. ± 217.	-164. ± 217.	180. ± 31.	67.8 ± .8	-.008 ±.007	1.3
3	420. ± 10.	3,938. ± 65.	39. ± 50.	78.9 ± 15.9	58.7 ± .5	-.010 ±.010	.91
4	490. ± 10.	4,687. ± 70.	553. ± 57.	93.3 ± 15.3	53.5 ± .5	+.006 ± .008	.86

where v is the beam velocity. Since the ratio c_5/c_2 was fixed to be 109.8, the mean lifetime τ of the 3p states of hydrogen is determined from the expression

$$\tau = \gamma^{-1} = (c_5 v/109.8)^{-1}. \tag{19}$$

Finally, the quantity of fundamental interest which can be obtained from Table 2 is the modulation amplitude, $M = c_4/c_1$. Eq. 12 of Section Two can be solved for the cross section ratio σ_1/σ_o in terms of the modulation amplitude M, the angular frequency of the fine structure splitting ω, the intrinsic polarization parameter g, the slit function parameters ε and δ, and the beam velocity v.

$$\frac{\sigma_1}{\sigma_o} = \frac{4(g-2) + (5+2g)\left[\dfrac{M\omega^2(\varepsilon^2-\delta^2)}{v^2\{\cos(\omega\delta/v) - \cos(\omega\varepsilon/v)\}}\right]}{4(g-2) + (4+7g)\left[\dfrac{M\omega^2(\varepsilon^2-\delta^2)}{v^2\{\cos(\omega\delta/v) - \cos(\omega\varepsilon/v)\}}\right]} \tag{20}$$

It should be pointed out that the beam velocity v, which appears in Eqs. 18, 19 and 20, is calculated from the beam energy downstream from the foil. That is, energy loss due to the passage of ions through the foil must be taken into account (29).

Before the results of these calculations can be presented and discussed, it is necessary to consider the sources of error and their significance in this experiment.

SOURCES OF ERROR

The determination of the relative magnetic substate cross sections of interest depends on measurements of the modulation amplitude, the slit function parameters, and the polarization parameter of the spectrometer. By far the largest uncertainty in the cross section determination is due to the uncertainty in the measurement of g, the polarization parameter. For this reason any systematic errors in the determination of the slit function parameters ε and δ may be neglected in computing the cross section ratio. The uncertainty in the modulation amplitude M, which contributes to the error in the cross section ratio σ_1/σ_o, can be calculated from the statistical uncertainties in the curve fitting parameters c_1 and c_4. Any systematic errors in the modulation due to a position dependent background or Stark mixing of the fine structure states of n = 3 caused by a small motional electric field are negligible compared to the relative statistical uncertainty in the modulation, which is typically 10% for the present data fits.

Since the relative uncertainty in g is 12%, any systematic error due to initial plane-polarization of the light source used in the measurement of g may be neglected in comparison. The light source was axially symmetric about the light beam axis and could be rotated while in use to verify that it was unpolarized or circularly

polarized; that is, its rotation did not influence intensity measurements.

One possible source of systematic error in the data runs which must be considered is Rutherford scattering of the beam atoms by the carbon nuclei in the carbon foil (30). The average angle of scattering of the beam by the foil results in a beam size which increases with distance from the foil. If the signal detection system samples only a fraction of the beam perpendicular to the beam axis due to the finite height of the spectrometer slits, then the fraction of beam sampled will decrease with increasing distance from the foil to the spectrometer. The Faraday cup, on the other hand, views the total beam. The effect would be to reduce the mean life calculated from the exponential decay of excited states measured in this way. This effect is negligible in the present experiment because the foil traverses a distance of only one inch during a data run. It can be important in lifetime measurements when the foil travels distances of the order of ten inches (30).

As mentioned in the previous section, the energy loss of the beam in passing through the foils must be taken into account in determining the velocity of the foil-excited hydrogen atoms. The tolerance on the original thickness of a 10 $\mu g/cm^2$ carbon foil is $\pm 4\ \mu g/cm^2$ and since the beam passes through two such foils, the total uncertainty in thickness is $\pm 8\ \mu g/cm^2$. This produces a

percentage uncertainty in velocity ranging from 1.% at 235 keV incident beam energy to .3% at 490 keV. Any velocity loss effects due to foil aging (31) are less than this amount and may be neglected. The uncertainty in the initial beam energy, determined by the calibrated voltmeter which reads acceleration voltage of the accelerator, is estimated to be less than 10 keV for all four data runs considered here. This estimate is based on an extrapolation of a calibration curve (32) of the voltmeter, which covered the range from 1 MeV to 2 MeV, using nuclear reaction threshold energies in this range. Molecular ion energies for the present work extend from 0.7 to 1.0 MeV.

In determining the exponential decay of the 3p states, background effects in the data runs may be important. A check was performed which verified that the background was small and constant during the data runs considered here. For this check the spectrometer was adjusted to pass radiation of approximately 1100 Å and the signal count rate at this wavelength was plotted versus the distance downstream from the foil. In the cases considered here, this background count rate was comparable to the value of the parameter c_3 obtained from the curve fit, and was approximately constant over the distance range of interest. Thus, the primary contributions to the error in the lifetime and fine structure energy splitting calculations came from the statistical uncertainty in the fitting parameter and from the error in the beam velocity.

RESULTS

Using Eq. 18 and the results in Table 2, the value of ΔE, fine structure splitting of the $3p_{3/2}$ and $3p_{1/2}$ energy levels of hydrogen, can be calculated. In addition, the lifetime τ of these excited states is given by Eq. 19 using the same data. Because the ratio of the quantities ΔE and τ was fixed at the theoretical value, the results presented here represent a verification of the fine structure splitting and the lifetime calculations. These results are summarized in Table 3, which also lists the energy loss of the ion beam in the foil at the beam energies used. The errors quoted for τ and ΔE represent one standard deviation uncertainty in these quantities. A comparison of the results of the present work with theory and other experiments is given in Table 4 for τ and ΔE.

The results of the calculation of σ_1/σ_0 for the various beam energies are listed in Table 5. Because this ratio theoretically can range from zero to infinity, it is more convenient to consider the ratio $(\sigma_1-\sigma_0)/(\sigma_1+\sigma_0)$. This latter parameter varies from -1 to +1 and is zero if $\sigma_1 = \sigma_0$. It is a convenient indicator of the orbital angular momentum magnetic substate alignment of hydrogenic atoms excited to L = 1 states by beam-foil collisions. Fig. 15 is a plot of this alignment parameter versus beam energy for the present experiment.

Table 3. Experimental results for the fine structure energy splitting and natural lifetime of the 3p states of hydrogen, from data fit at the various beam energies used.

Incident energy (keV)	Energy loss in foil (keV)	Velocity of foil excited atoms (in./nsec.)	Fine structure energy splitting E (kMH)	Lifetime (nsec)
235. ± 10.	-11.4 ± 4.5	.258 ± .006	3.29 ± .08	5.32 ± .13
338. ± 10.	-9.2 ± 3.7	.312 ± .006	3.36 ± .08	5.22 ± .12
420. ± 10.	-8.2 ± 3.3	.350 ± .005	3.27 ± .06	5.35 ± .09
490. ± 10.	-7.0 ± 2.7	.378 ± .004	3.22 ± .05	5.43 ± .08

Table 4. Lifetime and fine structure energy splitting of the 3p levels of hydrogen.

τ_{3p} (nsec)	Source	Method
5.8 ± .2	Bickel and Goodman (28)	Beam-foil
5.58 ± .13	Chupp et al. (31)	" "
5.41 ± .18	Etherton et al. (30)	" "
5.36 ± .06	Present study	Zero field beats
5.40	Bethe and Salpeter (1)	Calculation
$\Delta E\ (3p_{3/2} - 3p_{1/2}$: MH)		
3,280. ± 40.	Present study	Zero field beats
3,250.085 ± .013	Taylor, Parker and Langenberg (33)	Calculation

Table 5. Ratio of magnetic substate cross sections for the 3p states of hydrogen at various beam energies.

Beam energy per atom (keV)	σ_1/σ_o
235. ± 10.	1.32 ± .08
338. ± 10.	1.79 ± .22
420. ± 10.	2.4 ± .6
490. ± 10.	2.2 ± .4

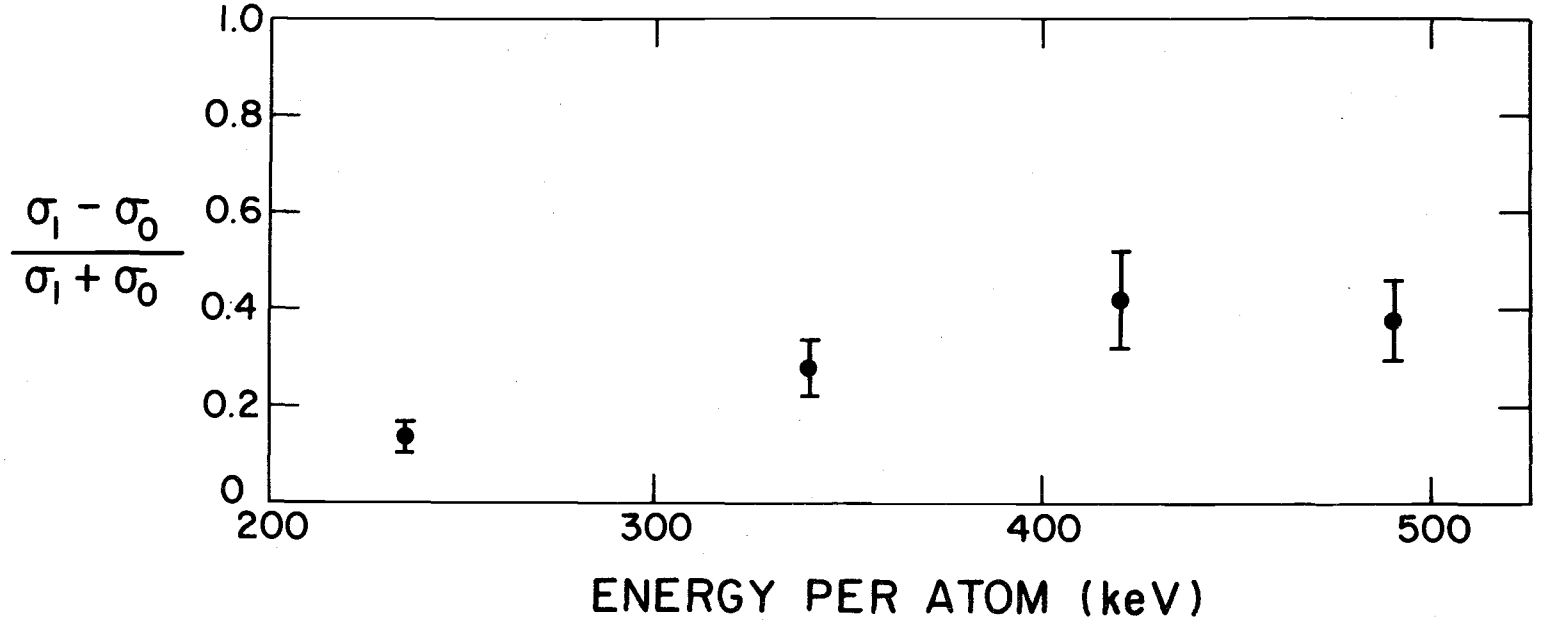

Fig. 15. $\sigma_1 - \sigma_o / \sigma_1 + \sigma_o$ for beam energies from 230 to 500 keV per atom.

DISCUSSION

This study demonstrates that the zero field beam-foil technique can provide a useful method of measuring fine structure energy splittings in excited atomic levels if the corresponding quantum beat wavelength is experimentally resolvable, and the relative magnetic substate cross sections of interest are significantly different.

The results of the present study which are of primary interest are the values of the orbital angular momentum magnetic substate cross section ratio given in Table 5 for various beam energies. A definite energy dependence of the σ_1/σ_o ratio is indicated. Unfortunately, there exists no detailed theoretical model for the beam-foil excitation process at the present time. Therefore, no comparison of these results with theory can be made here. However, the data obtained from this work as well as other zero-field experiments with different atomic energy level transitions at different beam energies should prove useful in testing any future theoretical models. In Table 6, a summary of all presently known σ_1/σ_o results is given. Clearly, it would be desirable to study these relative cross sections over a wider energy range to provide a more detailed description of the experimentally observed energy dependence.

A knowledge of the dependence of beam-foil excitation cross sections on principle quantum number, orbital angular momentum,

Table 6. σ_1/σ_o cross section ratio - summary of all presently known experimental results.

Beam energy per a.m.u. (keV)	Reference	Atom, excited level	σ_1/σ_o
50.	Sellin (22)	H, 2p	1. ± .2
117.	Andra (17)	He, 3^3p	.8 ± .1
133.	Andra (17)	H, n=4	> 1
150.	Sellin (22)	H, 2p	1. ± .2
235.	present study	H, 3p	1.32 ± .08
338.	present study	H, 3p	1.79 ± .22
420.	present study	H, 3p	2.4 ± .6
490.	present study	H, 3p	2.2 ± .4

magnetic substates and beam energy would be useful in testing theoretical models for the collision process. Experimental investigation of collision induced coherence between states of different orbital angular momentum is also essential to understanding the beam-foil interaction (9-13). From Stark-induced quantum beats experiments, it is possible to extract relative cross sections for excitation of orbital angular momentum states of opposite parity. The ratio σ_p/σ_s has been determined to be 4±1 for the n = 2 level of hydrogen at 200 keV beam energy per atom (17). The energy dependence of this ratio has not been investigated experimentally. Thus far, no experiments have been performed to determine the n dependence of the excitation cross sections.

BIBLIOGRAPHY

1. Bethe, H. and E. Salpeter. Quantum mechanics of one- and two-electron atoms. New York, Academic Press, 1957. 368 p.

2. Bashkin, S., ed., Beam foil spectroscopy. New York, Gordon and Breach, 1968, 180 p.

3. Garcia, J. D. Foil excitation mechanisms. Nuclear Instruments and Methods 90:295-298. 1970.

4. Bickel, W. S., et al. Multi-collisional molecular orbital model for the beam-foil interaction process. Nuclear Instruments and Methods 90:309-314. 1970.

5. Hughes, R. H., H. Dawson, and B. Doughty. Measurement of the lifetimes of the n=3 states of H by electron capture during H^+ impact on gases. Journal of the Optical Society of America 56:830-831. June, 1966.

6. Macek, J. Interference between coherent emissions in the measurement of atomic lifetimes. Physical Review Letters 23:1-2. July 7, 1969.

7. Bashkin, S. Beam foil spectroscopy. Applied Optics 7:2341-2350. December, 1968.

8. Heroux, L. Radiative lifetimes for uv multiplets of NII through NV. Physical Review 153:156-163. Jan. 5, 1967.

9. Macek, J. Theory of atomic lifetime measurements. Physical Review A 1:618-627. March, 1970.

10. Macek, J. Associate Professor, University of Nebraska, Department of Physics. Private communication. Corvallis, Oregon. May, 1971.

11. Andra, H. J. Zero-field quantum beats subsequent to beam-foil excitation. Physical Review Letters 25:325-327. August 10, 1970.

12. Andra, H. J. Quantum beats and level crossing after beam foil excitation. Nuclear Instruments and Methods 90:343-349. August 10, 1970.

13. Sellin, I. A., et al. Relative orbital and magnetic substate amplitudes in single-foil excitation of fast hydrogen atoms. Physical Review A 2:423-429. August, 1970.

14. Bickel, W. Electric-field and multiple-foil excitation experiments on beam-foil excited hydrogen atoms. Journal of the Optical Society of America 58:213-221. February, 1968.

15. Sellin, I. A., et al. Periodic intensity fluctuations of Balmer lines from single foil excited fast hydrogen atoms. Physical Review 184:53-63. August, 1969.

16. Sellin, I. A., et al. Stark perturbed Lyman-alpha decay in flight. Physical Review 188:217-221. December, 1969.

17. Andra, H. Stark-induced quantum beats in H Ly-alpha emission. Physical Review A 2:2200-2207. December, 1970.

18. Graves, P. W., et al. Operation of channeltron and spiraltron electron multipliers in the pulse saturated mode. Bendix Research Corporation Technical Applications Note 6902: 14 p. Ann Arbor, Michigan. May, 1969.

19. Samson, J. Techniques of vacuum ultraviolet spectroscopy. New York, John Wiley and Sons, 1967. 348 p.

20. Schmidt, K. and C. Hendee. Continuous channel electron multiplier operated in the pulse saturated mode. I. E. E. E. Transactions on Nuclear Science 13:100-111. June, 1966.

21. Johnson, M. C. and J. Svenson. Absolute quantum efficiency of a channeltron photomultiplier. Bendix Research Corporation Technical Note: 6 p. December, 1966.

22. Sellin, I. A., et al. Relative orbital and magnetic substate amplitudes in single-foil excitation of fast hydrogen atoms. Physical Review A 2:423-429. August, 1970.

23. Reference 1, p. 253.

24. Reitz, J. and F. Milford. Foundations of electromagnetic theory. 2d. Edition. Reading, Mass., Addison-Wesley Publishing Company, 1967. 435 p.

25. Rabinovitch, K. et al. A method for measuring polarization in the vacuum ultraviolet. Applied Optics 4:1005-1010. August, 1965.

26. Ramsey, N. Molecular beams. London, Oxford University Press, 1963. 453 p.

27. Bevington, P.R. Data reduction and error analysis for the physical sciences. New York, McGraw-Hill Book Company, 1969. 336 p.

28. Bickel, W. and A. Goodman. Mean lives of the 2p and 3 p levels in atomic hydrogen. Physical Review 148:1-4. August, 1966.

29. Northcliffe, L. Passage of heavy ions through matter. Annual Review of Nuclear Science 13:67-102. 1963.

30. Etherton, R. C., et al. Lifetimes of 3p, 4p, and 5p states in atomic hydrogen. Physical Review A2:2177-2179. December, 1970.

31. Chupp, E. L. Dotchin and D. Pegg. Radiative mean-life measurements of some atomic hydrogen excited states using beam-foil excitation. Physical Review 175:44-50. November, 1968.

32. Lefevre, H. and C. Burke. Calibration curve for generating voltmeter - U. of Oregon Accelerator data book. Eugene, Oregon, 1970.

33. Taylor, B., W. Parker and D. Langenberg. Determination of e/h, using macroscopic quantum phase coherence in superconductors: Implications for quantum electrodynamics and the fundamental constants. Reviews of Modern Physics 41: 375-496. July, 1969.

34. Abeles, F. Un theoreme relatif a la reflexion metallique. Comptes Rendus 230: 1942-1943. May, 1950.

APPENDIX

APPENDIX

Theory of the Measurement of the Intrinsic Polarization of the Spectrometer

This appendix develops the theory for the method (25) which was used to determine the intrinsic polarization of the spectrometer, as discussed in Section Four.

Given an unpolarized source of light at the entrance slits, this method assumes that the radiation emerging from the exit slits of the spectrometer is either unpolarized or partially plane polarized with the maximum of the electric (E) vector in a plane either parallel to, or perpendicular to the grating rulings (and thus the entrance and exit slits) of the spectrometer. This assumption should be good since the grating would be expected to polarize relative to its axis.

First, a plane reflecting surface is oriented in the exit beam of the spectrometer such that the angle of incidence is 45°. Two measurements of reflectance are taken: one with the plane of incidence perpendicular to the exit slit, the other with the plane of incidence parallel to the exit slit. Let I_V be the intensity of the component of radiation from the spectrometer having the E vector oriented parallel to the exit slit, and let I_H be the intensity of the component having the E vector oriented perpendicular to the exit slit. Define $g = I_V/I_H$. Let R_p be the reflectance at 45° angle of

of incidence for the intensity component with E vector oriented parallel to the plane of incidence, and R_s be the reflectance of 45° for the component of intensity with E vector oriented perpendicular to the plane of incidence. With the reflecting surface oriented so that the plane of incidence is perpendicular to the exit slit, the net 45° reflectance, R_1, is given by

$$R_1 = (I_V R_s + I_H R_p)/(I_V + I_H) \tag{A-1}$$

and when the plane of incidence is parallel to the slit, the net 45° reflectance, R_2, is

$$R_2 = (I_V R_p + I_H R_s)/(I_V + I_H) \tag{A-2}$$

Thus,

$$R_1 = (R_p + gR_s)/(1+g) \tag{A-3}$$

$$R_2 = (gR_p + R_s)/(1+g) \tag{A-4}$$

Abeles (34) has shown directly from Maxwell's equations that, for reflectance at the interface of two homogeneous, isotropic semi-infinite media, both having the same magnetic permeability, the following relationship holds.

$$R_p = R_s^2 \quad (\theta = 45°) \tag{A-5}$$

This relationship is independent of the optical constants of the media involved except that the medium of incidence (in this case a vacuum) is completely transparent. This relationship holds if the reflector is

opaque, homogeneous, and non-magnetic. Solving Eqs. (A-3)-(A-5) for g in terms of R_1 and R_2 gives

$$g = \frac{R_2[1+4(R_1+R_2)]^{\frac{1}{2}} - (R_2+2R_1)}{R_1[1+4(R_1+R_2)]^{\frac{1}{2}} - (R_1+2R_2)} \qquad \text{(A-6)}$$

It should be noted that measurements of g based on the above development agree with results from a more elaborate double reflectance method discussed in reference (25). This provides an experimental verification of the correctness of the above method.